Journal of Hydrology 400 (2011) 24–40

Contents lists available at ScienceDirect

Journal of Hydrology

journal homepage: www.elsevier.com/locate/jhydrol

The influence of conceptual model uncertainty on management decisions for a groundwater-dependent ecosystem in karst

Bibi R.N. Gondwe [a,*], Gonzalo Merediz-Alonso [b], Peter Bauer-Gottwein [a]

[a] Department of Environmental Engineering, Technical University of Denmark, Miljoevej, Building 113, DK-2800 Kgs. Lyngby, Denmark
[b] Amigos de Sian Ka'an, Calle Fuego No. 2, Manzana 10 SM 4, Cancún, Quintana Roo, 77500, México

ARTICLE INFO

Article history:
Received 2 December 2009
Received in revised form 22 November 2010
Accepted 19 January 2011
Available online 26 January 2011

This manuscript was handled by P. Baveye, Editor-in-Chief

Keywords:
Catchment modelling
Model structure
Equivalent porous medium
Aquifer
Sian Ka'an
Mexico

SUMMARY

Groundwater management in karst is often based on limited hydrologic understanding of the aquifer. The geologic heterogeneities controlling the water flow are often insufficiently mapped. As karst aquifers are very vulnerable to pollution, groundwater protection and land use management are crucial to preserve water resources and maintain ecosystem services. Multiple Model Simulation highlights the impact of model structure uncertainty on management decisions using several plausible conceptual models. Multiple Model Simulation was used for this purpose on the Yucatan Peninsula, which is one of the world's largest karstic aquifers. The aquifer is the only available fresh water source for human users and ecosystems on the Peninsula. One of Mexico's largest protected areas, the groundwater-dependent Sian Ka'an Biosphere Reserve (5280 km^2) is fed by the aquifer's thin freshwater lens. Increasing groundwater abstractions and pollution threatens the fresh water resource, and consequently the ecosystem integrity of both Sian Ka'an and the adjacent coastal environment. Seven different catchment-scale conceptual models were implemented in a distributed hydrological modelling approach. Equivalent porous medium conceptualizations with uniform and heterogeneous distributions of hydraulic conductivities were used. The models demonstrated that Sian Ka'an's wetlands are indeed groundwater-fed. The water quantities in the wetlands and the flooding dynamics are determined by the larger groundwater catchment. The overall water balance for the model domain showed that recharge constitutes 4400 ± 700 million m^3/year. Of this, 4–12% exits as overland flow, and 88–96% exits as groundwater flow. Net groundwater outflow from the model domain to the north via the Holbox fracture zone appears as an important cross-basin transfer between regions of the Peninsula. Probability maps of Sian Ka'an's catchment were obtained through automatic calibration and stochastic modelling. Groundwater travel time zones were calculated based on different calibrated effective porosities. The spatial modelling results highlight the impact of regional-scale structures on the flow field and transport times.

1. Introduction

The need to provide water, both for human demands and for ecosystems, is increasingly being recognized worldwide, placing interaction between groundwater and surface water in political and scientific focus (Kilroy et al., 2005; Eamus and Froend, 2006; Münch and Conrad, 2007; Krause et al., 2007). Terrestrial groundwater-dependent wetland ecosystems are some of the world's most productive ecosystems, and therefore the target of protection and restoration efforts. Groundwater-dependent ecosystems in karst are particularly vulnerable to pollution because of rapid groundwater flow and contaminant transport in karst aquifers.

In Mexico, one of the largest protected areas is a groundwater-dependent ecosystem in karst. The 5280 km^2 Sian Ka'an Biosphere Reserve on the Yucatan Peninsula includes large wetlands taking up about one third of the area (Fig. 1). Their rich ecosystem diversity and recreational value is internationally and regionally valued, and the area is listed as a Ramsar site and a UNESCO World Heritage site. The wetlands are fed by a thin fresh groundwater lens, only up to 100 m thick (Gondwe et al., 2010b), which effectively is the only fresh water resource available on the Yucatan Peninsula.

Peninsula-wide, groundwater demands and groundwater pollution problems are growing. Both in northwestern Yucatan Peninsula (Escolero et al., 2000) and along the eastern coast (Fideicomiso Para la Promoción Turística de la Rivera Maya, 2004), significant and rapid increases in population density and water demands are taking place, partly due to an expanding tourism industry in the east. Groundwater pollution in Yucatan State has been documented by Pacheco et al. (2001), while agricultural activities are intensifying in the state of Quinana Roo (Mazzotti et al., 2005). Wastewater is typically re-injected into the Peninsular aquifer, and often does not undergo prior treatment (ASK, 2003;

* Corresponding author. Tel.: +45 4525 1570; fax: +45 4593 2850.
E-mail addresses: bibi.neuman@gmail.com (B.R.N. Gondwe), gmerediz@amigosdesiankaan.org (G. Merediz-Alonso), pbg@env.dtu.dk (P. Bauer-Gottwein).

0022-1694/$ - see front matter © 2011 Elsevier B.V. All rights reserved.
doi:10.1016/j.jhydrol.2011.01.023

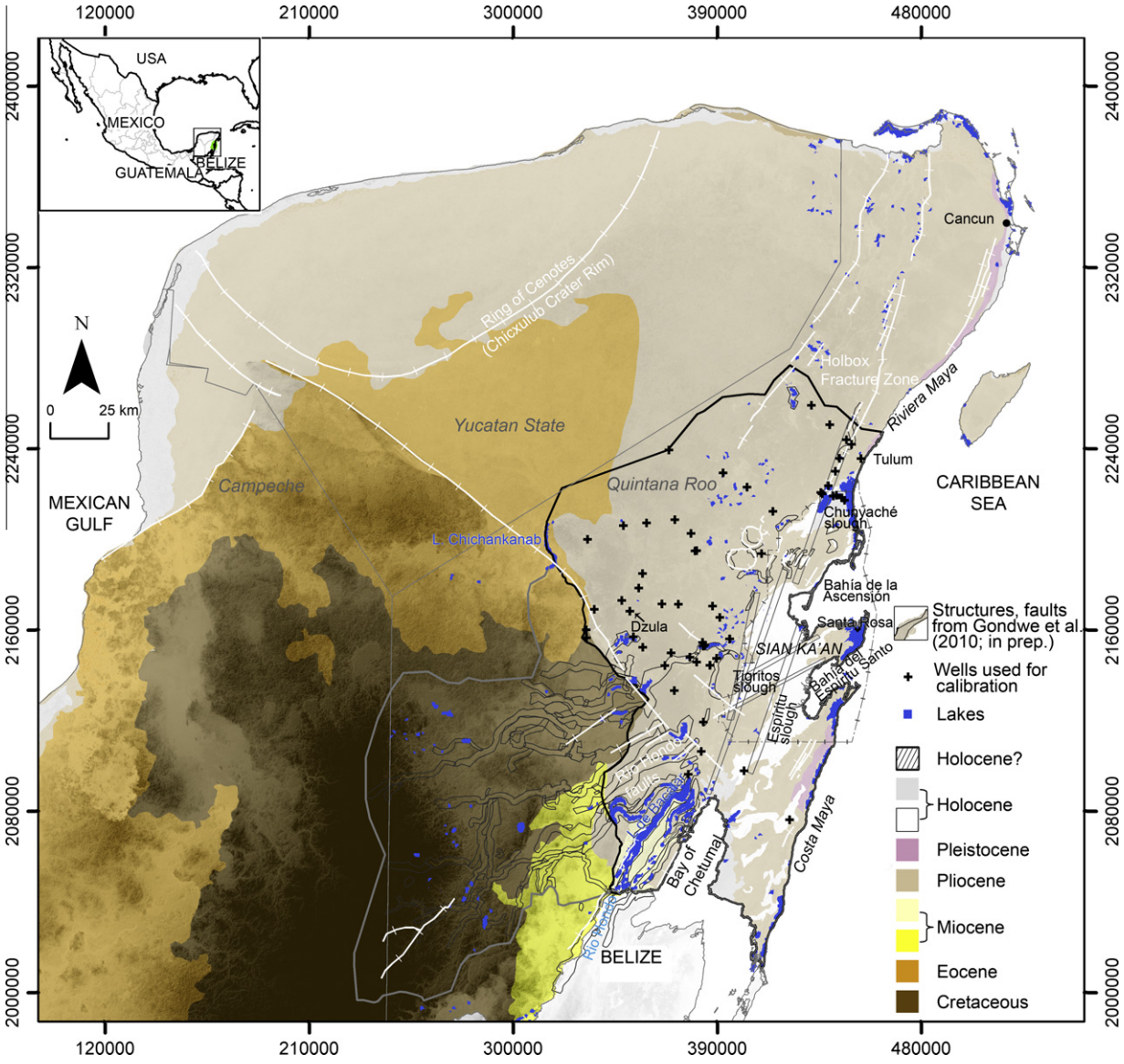

Fig. 1. Geology of the Yucatan Peninsula, modified from SGM (2007). Oldest sedimentary rocks dated as Cretaceous instead of Paleocene, based on Schönian et al. (2005) and Lopez-Ramos (1975) (Ichaiche Formation). Topography from SRTM (USGS, 2006) overlain as grey-scaled transparent. Study area outlined with thick grey polygon, model domain outlined as thick black polygon. Coordinates are UTM zone 16 N, WGS84 datum and ellipsoid. (For interpretation of the references to colour in this figure legend, the reader is referred to the web version of this article.)

Beddows 2002; Beddows et al., 2005; Marín et al., 2000; Krekeler et al., 2007). Thus, the tradeoff between human water use and ecosystem water use appears as a major groundwater management problem on the Yucatan Peninsula.

To manage the water resources of the groundwater-dependent ecosystem soundly, it is necessary to delineate its catchment. Distributed hydrological modelling is the method of choice, but in the highly heterogeneous karst aquifers, catchment delineation poses a particular challenge. A karst aquifer is a triple porosity medium, consisting of the rock matrix (intergranular porosity), the fractures and bedding planes and the karstic conduits (White, 1999). Most karstic groundwater flow takes place in the conduits, whereas the matrix is the prime compartment for water storage (Atkinson, 1977; Worthington, 2003). The unknown heterogeneities make it difficult to predict karstic groundwater flow accurately. Groundwater management initiatives, such as land use zonation, are therefore often made based on limited hydrogeologic understanding of the aquifer.

Conceptual model uncertainty can be addressed using Multiple Model Simulation. Here we use the term conceptual model to signify the schematic representation of the real system. Thus, the hydrogeological interpretation, the physical processes included in the model, their mathematical formulation, boundary conditions and initial conditions are included in a conceptual model. The numerical scheme is considered a way of realizing the conceptual model, and is hence not a part of the conceptual model. The impact of uncertainty in the conceptual model is usually far greater than the impact of any model parameter uncertainty (Neuman and Wierenga, 2003; Højberg and Refsgaard, 2005). In Multiple Model Simulation a number of different plausible conceptual models are formulated and calibrated. Based on validation tests, models are accepted or rejected. All accepted models are subsequently used for prediction and uncertainty assessment (Refsgaard et al., 2006). Multiple Model Simulation increases the robustness of model predictions and yields explicit analyses of the consequences of using alternative models. The limitations of the Multiple Model Simulation approach are that the selection of conceptual models is necessarily subjective and often incomplete. Important plausible conceptual models may be left out, and it is not possible to quantify the probability of each alternative model (Refsgaard et al., 2006, 2007).

Numerically, karst aquifers may be represented in various ways. Here we consider only distributed models. Distributed hydrological modelling studies that take all three aquifer continua into account are limited (e.g. Cheng and Chen, 2005). However, a relatively common numerical modelling method is to consider two continua, the matrix and the conduits, and include an exchange component between the two (e.g. Birk et al., 2003; Liedl et al. 2003). Flow in the larger apertures may be turbulent, while the flow in the matrix is laminar. These double-continuum models are physically sound but also complex and computationally expensive. Problems occur in the parameterization of the highly variable caves (e.g. cave location, course, roughness, dimensions) and in quantifying the exchange between the continua, particularly at larger scales. Parameter uncertainty can have significant impacts on the models since slight changes in some cave parameterizations can notably change model output (Peterson and Wicks, 2006), and the exchange between conduits and matrix is still little understood (Martin and Screaton, 2001; Bauer et al., 2003; Peterson and Wicks, 2005). Catchment-scale applications of double-continuum models are limited by the high computational load. Moreover, sufficiently detailed data are typically not available for large areas.

The simplest way of modelling a distributed karst aquifer is to assume that the aquifer can be represented by an equivalent porous medium. This assumption is reasonable if the numerical cell size is 'large enough', i.e. equals or exceeds a "Representative Elementary Volume" (REV). The hydraulic conductivity (K) assigned to a cell represents the combined effect of matrix, fractures, and conduits within the cell. In a few cases the equivalent porous medium approach has been successful (e.g. Larocque et al., 1999, 2000; Scanlon et al., 2003), but it is also often criticized as too simplistic to represent karst flow (e.g. Kovacs et al., 2005). By using the equivalent porous medium approach, important features that characterize karst aquifers are ignored, e.g. the duality of infiltration and the duality of discharges (Kiraly, 2003). Important conduits may in some equivalent porous medium models be represented as zones with a higher K than the matrix, and there is exchange between the matrix and the 'conduits' (zones of higher K). This approach still models only laminar flow all over the model domain, but incorporates some of the important heterogeneity of karst aquifers. Assigning such "block permeabilities" to different zones gives a higher accuracy than not including zones, if the zonation and assignment of values is reasonably reliable (Durlofsky, 1992). The approach of assigning higher K to known conduit areas in an equivalent porous medium model has been successfully used by e.g. Knochenmus and Robinson (1996), Lindgren et al. (2005), Worthington (2009) and Kiraly (2003). This simplified approach is applicable especially for regional-scale studies.

The present study aims to illustrate the effects of model structure uncertainty on management decisions in karst. For the catchment of the Sian Ka'an Biosphere Reserve we test different conceptual models of the area using equivalent porous medium approaches with and without zones of higher K. Models are accepted or rejected based on quantified fluxes and model fits to measured heads. The accepted hydrological models are then used to delineate the catchment that contributes with groundwater to Sian Ka'an using stochastic modelling. The implications for groundwater management are discussed.

2. Methods and data

2.1. The study area

The study area is the 35,000 km^2 tentative groundwater catchment of the Sian Ka'an Biosphere Reserve (SKBR), located in Quintana Roo, Mexico (Fig. 1). The study area was delineated based on topographic divides. By doing this it was assumed, as a first-order approximation, that topographic divides coincide with groundwater divides. The part of the study area's boundary just north of Tulum was perpendicular to the coast, and was not delineated based on topography, but based on an assumed flow line. This assumed boundary was far enough away from SKBR to ensure that areas further north would not contribute groundwater to the Reserve. The groundwater head data presently available for the peninsula are in agreement with these tentative catchment boundaries. Geochemical findings of Perry et al. (2002) support the water divide at Lake Chichankanab.

Average precipitation ranges from 840 to 1550 mm/year. Three quarters of the precipitation falls between May and October (unpubl. climate data from Comisión Nacional del Agua). A spatial estimate of actual evapotranspiration, using the 'triangle method' and MODIS data, showed that average recharge equals about 17% of mean annual precipitation in the study area (Gondwe et al., 2010b). The area is subject to tropical storms. Average monthly temperatures range from 23 to 27 °C. Soil cover is limited and most of the area is covered by 15–30 m tall semi-evergreen forest (Sánchez-Sánchez and Islebe, 2002; INEGI, 1997). Sian Ka'an contains coastal savannas, swamps, marshes, and mangrove, in addition to tropical forests, and hosts endangered and endemic species (Morales Barbosa, 1992; Mazzotti et al., 2005). From August 2006 to February 2008 the wetland extent varied between 1067 km^2 and 2588 km^2, owing to natural variations in inflow and to effects of extreme rainfall events. Smallest extent was in May and largest in December in a typical year (Gondwe et al., 2010a).

The Yucatan Peninsula consists of limestones, dolomites, and evaporites reaching thicknesses of >1500 m (Weidie, 1985). The surficial sedimentary rocks span Upper Cretaceous to Holocene in age, and are generally nearly horizontally layered and off-lapping, with gradually younger carbonates deposited towards the Peninsula margins (Lopez-Ramos, 1975; SGM, 2007; Schönian et al., 2005) (Fig. 1). The geology is poorly constrained in the southern and central Peninsula due to few exposures and difficulties in dating the sedimentary rocks through biostratigraphy (Kenkmann and Schönian, 2006). The Yucatecan carbonates are heavily karstified and host abundant caves, including the world's longest underwater cave system (http://www.caves.org/project/qrss/qrlong.htm; http://www.caverbob.com/uwcave.htm). Extensive cave systems have mainly been mapped in the northern part of Sian Ka'an, along the coast north of SKBR, and up to roughly 10 km inland. This is likely a result of sampling bias, as most cave divers live in this area, thus concentrating most exploration efforts there (Beddows, 2004). However, the possibility also exists that the extensive cave systems are related to the Pleistocene geology only deposited in this area (Neuman and Rahbek, 2007 and references herein). In neighboring Belize, cave development in the Tertiary sedimentary rocks is practically unknown, despite an abundance of mapped cave systems in other geologies (Miller, 1996).

The study area contains a notable topographic contrast. The topographic relief is flat in the northern and coastal parts of the Pliocene geology (elevations 0–20 meters above mean sea level (mamsl)), whereas the south-southwestern, mainly Cretaceous, areas have an undulating relief with cone-karst landforms (elevations 50–340 mamsl). In between there is a transition zone with moderately undulating relief (20–50 mamsl). A similar divide exists in the groundwater phreatic surface (Gondwe et al., 2010b). The Pliocene area has a very low hydraulic gradient (3–7 cm/km) with relatively small water level variations (5–40 cm within a year). This indicates a high transmissivity. In contrast, the Cretaceous geology has perched aquifers, and higher hydraulic gradients (10–190 cm/km). Water level variations have not been recorded here. Geochemistry shows groundwater dominated by gypsum in

the Cretaceous part of the study area, which supports a lower transmissivity in this geology (Gondwe et al., 2010b). The main groundwater flow direction, deduced from phreatic surface measurements, is SW–NE from the Cretaceous area to the Pliocene area, and W–E towards the coast within the Pliocene area.

In the Pliocene geology, the fresh groundwater forms a lens floating on top of saline water. The Dupuit–Ghyben–Herzberg model can be used to describe the thickness of the freshwater lens on a regional scale in the study area's Pliocene geology (Gondwe et al., 2010b). However, only 100 m from the coast at Tulum, Beddows (2004) showed that the freshwater lens is 4.6 to 7 m thick. This is thicker than predicted from the Dupuit–Ghyben–Herzberg model. As the presence of conduits violates the assumptions of the Ghyben–Herzberg principle, its applicability at the local scale is limited. Beddows (2004) suggested the thicker freshwater lens at the coast may be due to outflow restrictions. Coastal caves explored by cave divers north of Tulum are smaller than inland caves. Moreover, they are often parallel to the coast because they developed along joints (Smart et al., 2006). In the Cretaceous hilly area saline intrusion has not been documented, and is not reflected in the geochemistry (Gondwe et al., 2010b; Perry et al., 2009). Thus, the thickness of the fresh aquifer in this area is unknown.

Important physiographic features characterize the study area. The Río Hondo faults are a series of sub-parallel faults, trending SSW–NNE, and located in the southern part of the study area (Fig. 1). They have not been mapped in detail but fault-guided lakes are a surface expression of the faults (e.g. Laguna de Bacalar). The Río Hondo faults are normal faults with the downthrown side to the east. They have shaped the Caribbean coastline in the study area, and sub-parallel horst and graben systems are present offshore (Rosencrantz, 1990). Another fault system is located in the northern part of the study area – the Holbox fracture zone, also trending SSW–NNE. Its southern terminus is not well determined but possibly the Holbox and Río Hondo fault systems intersect (Southworth, 1985). Sharp linear wetland boundaries within Sian Ka'an have been proposed to be fault-controlled (Gondwe et al., 2010a), outlining additional possible sub-regional faults within Sian Ka'an between the two main regional fault systems.

Regional-scale structures have been delineated within the study area using remote sensing imagery and topographic elevation data (Gondwe et al., submitted for publication) (Fig. 1). Most of these structures are sub-parallel to the Río Hondo faults and may constitute a part of this system. Possibly these structures may be regional high-permeability zones. Airborne electromagnetic investigations have been carried out over the structures but could not definitively determine their hydraulic character because of a shallow, highly conductive geologic layer (Gondwe et al., submitted for publication). Seasonal surface water runoff takes place in these structures, but infiltrates into the aquifer before reaching the coast (SGM, 2007; Pope and Dahlin, 1989). The shallow geologic layer with high electrical conductivity and likely high clay content is the proposed reason for the reduced infiltration capacity over the structures (Gondwe et al., 2010b). This layer is probably discontinuous, due to erosion following its deposition (Pope et al., 2005; Kenkmann and Schönian, 2006; Urrutia-Fucugauchi et al., 2008). Despite its general presence throughout the hilly area and transition zone the layer does not appear to inhibit rapid infiltration to the aquifer at the regional scale. This is confirmed by rapid groundwater level responses to local rainfall (Gondwe et al., 2010b).

Previous hydrogeologic, geologic and hydrologic studies of the area are limited. Beddows (2003, 2004) and Beddows et al. (2007) studied cave hydrology on a local scale in Riviera Maya. Smart et al. (2006) and Supper et al. (2009) investigated the cave systems in the same area using direct inspection and airborne geophysical methods, respectively. The geology of a section in the southern part of the study area was characterized by Schönian et al. (2004, 2005) and Kenkmann and Schönian (2006), whereas geochemistry was investigated by Perry et al. (2002, 2009) on a regional scale. Hydrologic dynamics of the Sian Ka'an wetlands were investigated by Gondwe et al. (2010a), and regional-scale multidisciplinary field investigations of the tentative catchment were carried out by Gondwe et al. (2010b, submitted for publication), as an antecedent to the hydrological modelling presented in this paper. Hydrological modelling of Sian Ka'an's catchment has not been carried out in any previous studies.

Based on the findings of Gondwe et al. (2010b), the Pliocene geology of the study area can be considered one continuous aquifer, with a clearly defined lower level. The relation between this aquifer and any aquifer in the Cretaceous geology is undetermined. The nature and magnitude of any groundwater exchange between the Cretaceous area with the low transmissivities and the Pliocene area with the high transmissivities is not known. In addition, data on regional groundwater heads in the Cretaceous area are limited to three measurement points in the hilly area and eight in the transition zone, and it is not clear whether some of these are connected to perched aquifers. Moreover, the thickness of the freshwater aquifer in the Cretaceous area is unknown. Therefore, only the Pliocene part of the study area was simulated with a distributed hydrological model. The effects of the Cretaceous geology aquifer were represented as lumped boundary inflows. The model area of the distributed model was outlined based on geological boundaries from SGM (2007) and the 50 mamsl topographic contour line, as it was assumed that the rugged topography >50 mamsl near Lake Chichankanab did not belong to the generally more smooth Pliocene geology. Outside the delineated model area, the water levels were much higher than the 0.5—3 mamsl that characterize the Pliocene area aquifer. The total area of the distributed model was 21,000 km^2 (Fig. 1).

2.2. Design of the numerical hydrological models

An equivalent porous medium modelling approach was chosen because of the regional scale of the model area. Different conceptual models were developed based on the general knowledge and hydrogeological database of the study area. The conceptual models differed with respect to two main criteria: (A) Whether there is flow between the Cretaceous and the Pliocene area and (B) whether the structures and faults delineated in Gondwe et al. (submitted for publication, 2010a) are regional-scale zones of higher permeability. Consequently, four conceptual models were first set up and compared (Fig. 2): Model (1) No inflow from the Cretaceous area, and hydraulic conductivity (K) of the structures equal to that of the matrix. Model (2) Same as Model 1 but with structures having a different K than the surrounding equivalent porous medium matrix. Model (3) With inflow from the Cretaceous area to the discretized model domain. K of structures equals that of the matrix. Model (4) Same as Model 3, but with structures having a different K than the matrix.

The coupled surface-water/groundwater finite-difference code MIKE SHE (Refsgaard and Storm, 1995; Graham and Butts, 2006) was used. Darcian flow was assumed throughout the saturated zone. Grid cell size was 1×1 km^2 and hydraulic conductivity was assumed to be isotropic. The aquifer was assumed unconfined throughout the model domain. Mainly, steady state conditions were analysed. The unsaturated zone was disregarded in the model setup. Fast infiltration of recharge directly into the aquifer is considered a valid assumption for the average conditions represented by the steady state models. The saturated zone was modelled as one computational layer, resulting in a two-dimensional (2-D) simulation of groundwater flow.

The top of the aquifer was set as the topographic level obtained from the Shuttle Radar Topography Mission (SRTM) (USGS, 2006),

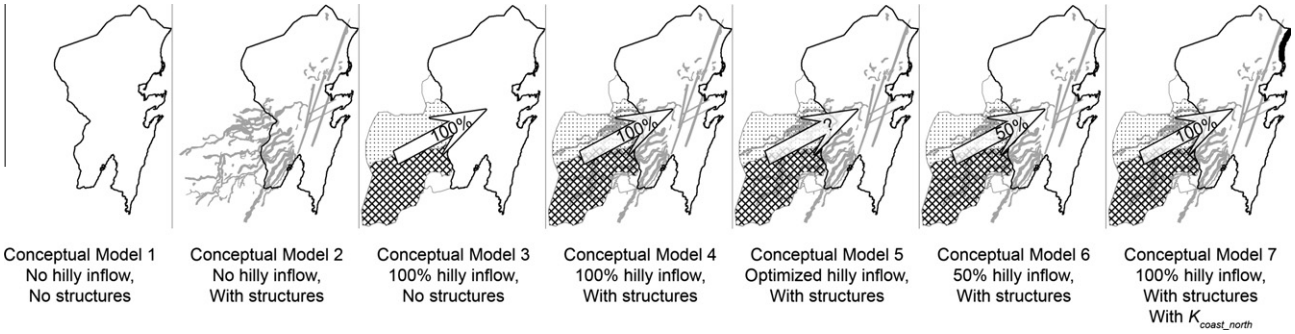

Fig. 2. The different conceptual models used in the Multiple Model Simulation.

resampled to the 1 km^2 grid. The simulated extent of overland flow was sensitive to topographic level. Moreover, the SRTM may measure to top of canopy instead of ground level. Therefore, the 2-percentile topographic value within each 1 km^2 grid cell was used as the topographic level. The simulated extent of flooding was then similar to that observed from remote sensing data (Gondwe et al., 2010a). A few coastal cells with topography <0 mamsl at some narrow coastal land tongues at the extremes of the model area were removed from the model domain, since they showed inflow from the sea in all modelling experiments.

The lower level of the aquifer was defined by using the Dupuit–Ghyben–Herzberg principle (Vacher, 1988) to convert modelled freshwater heads to depths to the halocline. This modelled depth to the halocline corresponded well with measured values obtained from time-domain electromagnetic measurements (root mean square error (RMSE) = 10.3 m (Fig. 3), which is in the same range as the uncertainty of the measurements (5–15 m, Gondwe et al., 2010b). At the coast, the lower level was set to −4.6 mamsl based on measurements in Beddows (2004). Next to the coastal cells minimum depth was set to −14.3 mamsl, based on Dupuit–Ghyben–Herzberg computations.

Boundary conditions were set to fixed head = 0 mamsl at the coast. Elsewhere, the Conceptual Model 1 had zero flux boundaries. The Conceptual Models 3 and 4 were given inflow (flux) boundaries near the Cretaceous area (see below). Conceptual Models 2 and 4 further had a fixed head boundary of 0.4 mamsl at the Holbox fracture zone. This fixed head value was obtained from neighboring water level measurements. Model sensitivity to uncertainty in this parameter was investigated by adding or subtracting an estimated standard deviation, σ_{Holbox_bound}, of 4 cm (Gondwe et al., 2010b) to/from the fixed head boundary, and calibrating these model scenarios. Discharge thus took place along the coast via the saturated zone and overland flow, and could also take place through the Holbox fracture zone, when structures were included. Discharge through groundwater abstractions were not included in the model due to lack of data. Hydrological modelling studies of the largest abstractions in Quintana Roo – at Cancun (outside the model area) have shown that even such relatively large abstractions (1.9 m^3/s distributed over 70 km^2) do not cause appreciable modification of the groundwater heads, because of the high transmissivity of the Pliocene aquifer (Charvet, 2009).

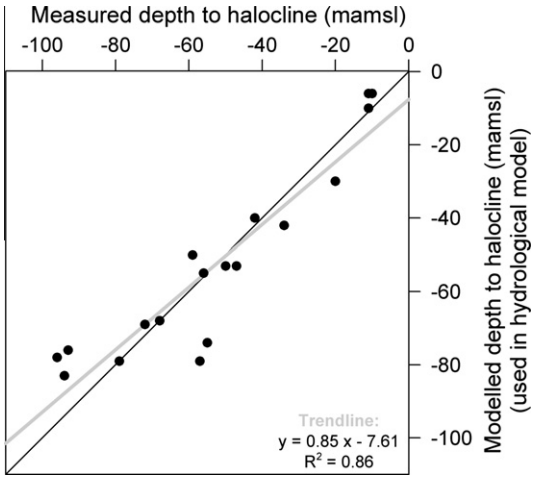

Fig. 3. Measured depth to halocline vs. the modelled depth to halocline, estimated using the Dupuit–Ghyben–Herzberg relation and modelled groundwater heads.

Spatial estimates of yearly average recharge from Gondwe et al. (2010b) were used directly in the model (mean: 0.5 mm/day, maximum: 1.8 mm/day, minimum: −2.3 mm/day within the model area). Model sensitivity to uncertainty in this parameter was investigated using scenario analysis, by adding or subtracting the standard deviation of the recharge, σ_R, to the recharge estimate, and calibrating these models. σ_R was estimated as $\sqrt{(\sigma_P^2 + \sigma_{ETa}^2)}$, where P is precipitation and ET_a is actual evapotranspiration. σ_P was estimated by comparing uncorrected precipitation estimates from Tropical Rainfall Measurement Mission (TRMM) (product 3B43) with precipitation data from 23 gauge stations within the study area. The estimated σ_P was 0.04 mm/day (=15 mm/year). An estimate of σ_{ETa} was obtained from data in Stisen et al. (2008). Our ET_a estimate was derived with similar methods as in Stisen et al. (2008), albeit with data from another remote sensor. Stisen et al. (2008)'s RMSE estimate (41.45 W/m^2 = 1.5 mm/day) is in the same order of magnitude as that obtained by most other authors, also cited in Stisen et al. (2008). The RMSE estimate was valid for daily estimates, and was re-calculated to the error of the yearly average ET_a by dividing it with the square root of the number of samples in a year $\left(\sqrt{365}\right)$, yielding an σ_{ETa} of 0.08 mm/day (=29 mm/year). The resulting estimate of σ_R was 0.09 mm/day. Spatial uncertainties for the recharge were not taken into account, as the spatial variation in the estimates of both ET_a and the precipitation is considered quite reliable. Moreover, synthetic modelling experiments indicate that the shape of groundwater catchments is influenced more by the uncertainty of the mean recharge than by the uncertainty of its spatial pattern (Hendricks Franssen et al., 2004).

To estimate the inflow from the Cretaceous area to the model domain (Models 3 and 4), surface water catchments of automatically delineated rivers were outlined based on topographic data using the software ILWIS 3.3 Academic (ITC, 2005). To a large extent the delineated rivers correspond to the structures connecting the Cretaceous area and the domain (Gondwe et al., submitted for publication). The underlying assumption was that groundwater divides in the hilly area would correspond with surface water divides. It appears reasonable to assume that at least part of the recharge in the hilly area generates surface water flow, given the

presence of a shallow low-permeability layer in this area, and the existence of swamps and ephemeral rivers (Gondwe et al., 2010b). Three main surface water catchments, consisting of sub-catchments connected by the rivers/structures, were obtained. They largely covered the Cretaceous part of the study area (Fig. 4). The surface water catchments termed 'North' and 'South' were used in the modelling. The surface water catchment 'Bacalar' appeared to discharge into the Río Hondo River on the boundary of the model domain, and was therefore not included. Average annual recharge of each 'North' and 'South' surface water catchment was calculated from the spatial recharge estimate. These values (in m^3/s) were then assigned as boundary inflow to the sections of the boundary, where the structures of the 'North' and 'South' catchments intersected the boundary. In Conceptual Models 3 and 4, 100% of the calculated recharge was used as inflow (42.9 m^3/s and 57.1 m^3/s for 'North' and 'South', respectively). The Conceptual Models 5 and 6 were introduced to investigate the sensitivity of the model to uncertainty in this inflow parameter. The percentage of inflow was included as a calibration parameter in Conceptual Model 5. Since the resulting difference between Conceptual Models 4 and 5 was minor, 50% of the calculated recharge was used as inflow in Conceptual Model 6, to study the influence of changing inflow on the model results.

The Preconditioned Conjugate Gradient solver (Hill, 1990) was used in the simulation for the saturated zone component. The overland flow was modelled using the diffusive wave approximation, with a Strickler/Manning law applied to the friction slopes, and the Successive Over-Relaxation solver of MIKE SHE. Manning's $M = 10\ m^{1/3}/s$ was applied to represent the friction losses due to micro-topography and the heavy vegetation of the Sian Ka'an wetlands. On a standard PC (Intel Pentium 4, 2.6 GHz, 1 GB RAM), the CPU time for running the model was approximately 1 min per simulated year, when the overland component was enabled.

2.3. Model calibration

The models were calibrated in steady state. Calibration was carried out using automatic inverse calibration. *K*-values (K_{matrix}, K_{struct}) were adjusted with the goal of minimizing the mean square error (MSE) between modelled and measured groundwater heads at 59 wells located within the model domain. Head data were a temporal average of the values presented in Gondwe et al. (2010b); roughly two wet and two dry season measurements. Estimated uncertainty on the measured values was ±4 cm based on average GPS error. The error due to time variation between head measurements was estimated to have its upper bound at ±13 cm, but in reality to probably be much lower, because the temporal measurements have some correlation. Uniform uncertainty was assumed on all water level measurement points given that the same measurement method and same temporal sampling was applied to all. Therefore, all points were weighted equally in the calibration. Structures and faults were assumed regionally connected (Fig. 5). Lindgren et al. (2005) assumed the same in their equivalent porous medium model of another karst region. The K_{struct} was not differentiated spatially. The literature (e.g. Liedl et al., 2003) indicates that

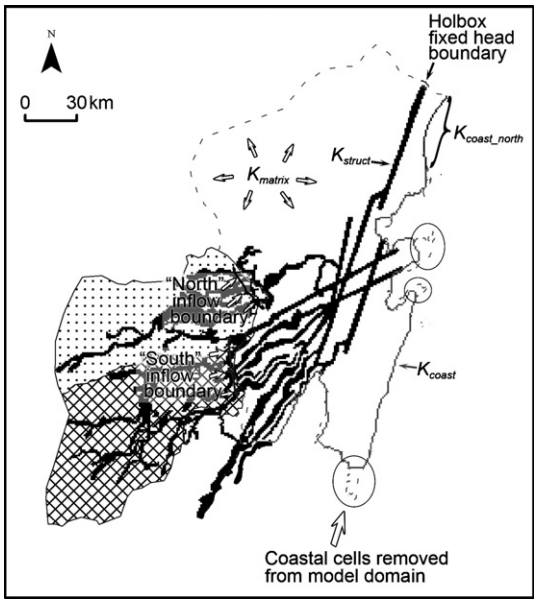

Fig. 5. Distribution of *K*-values in the models, and location of boundaries.

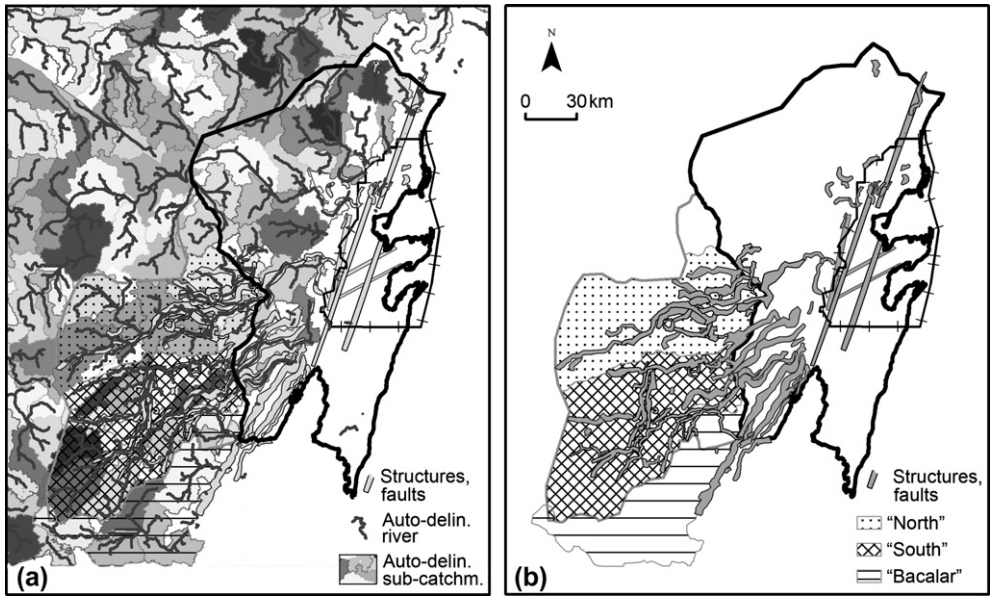

Fig. 4. (a) Automatically delineated surface water catchments in the hilly area and (b) the overall catchments used to estimate inflow through the boundary from the hilly Cretaceous area. Structures and faults from Gondwe et al. (submitted for publication, 2010a).

Table 1
Calibration results and selected model outputs for the conceptual models investigated. MSE = mean square error; OL: overland flow; SZ: saturated zone flow; SKBR: Sian Ka'an Biosphere Reserve; structs.: structures and faults, diff.: different. The two models giving the smallest MSE are marked in bold.

Conceptual model:	No hilly inflow, no structures	No hilly inflow, with structures	100% hilly inflow, no structures	100% hilly inflow, with structures	Hilly inflow optimized, with structures	50% hilly inflow, with structures	K_{coast_north} and 100% hilly inflow, with structures
MSE [m^2]	0.2381	0.1393	0.1422	0.1163	0.1162	0.1245	0.1086
K_{coast} [m/s]	0.048	0.011	0.110	0.059	0.065	0.038	0.060
K_{coast_north} [m/s]	–	–	–	–	–	–	0.440
K_{matrix} [m/s]	0.71	0.49	0.94	0.61	0.66	0.52	0.95
	[0.61; 0.83]	[0.31; 0.78]	[0.93; 0.95]	[0.38; 0.97]	–	[0.32;0.85]	[0.36;2.59]
$K_{structs}$ [m/s]	–	26.86	–	18.79	15.75	17.29	1.03
	–	[16.40; 43.98]	–	[5.13; 68.84]	–	[6.87; 43.51]	[0.26;4.16]
Calibrated (optimized) inflow	–	–	–	–	105.3%	–	–
MSE with OL [m^2]	0.2208	0.1647	0.1336	0.1160	–	0.1809	0.1047
$\frac{OL\_Outflow\_al\_domain}{SZ\_Outflow\_all\_domain}$ [% and OL outflow in m^3/s]	11.7%	42.4%	5.7%	10.3%	–	16.8%	7.8%
	(12.5 m^3/s)	(19.4 m^3/s)	(11.9 m^3/s)	(16.7 m^3/s)	–	(24.6 m^3/s)	(15.0 m^3/s)
$\frac{SZ\_Outflow\_SKBR}{SZ\_Outflow\_all\_domain}$ [% and SKBR SZ outflow in m^3/s]	49.5%	47.4%	42.9%	47.0%	–	46.5%	42.9%
	(52.7 m^3/s)	(21.7 m^3/s)	(89.5 m^3/s)	(76.2 m^3/s)	–	(68.1 m^3/s)	(82.9 m^3/s)
$\frac{OL\_Outflow\_SKBR}{SZ+OL\_Outflow\_all\_domain}$ [%]	9.2%	29.6%	4.2%	7.3%	–	11.7%	5.2%
Within SKBR only: $\frac{OL\_Outflow}{SZ\_Outflow}$ [% and SKBR OL in m^3/s]	18.5%	62.4%	9.8%	15.5%	–	25.2%	12.2%
	(9.8 m^3/s)	(13.6 m^3/s)	(8.7 m^3/s)	(11.8 m^3/s)	–	(17.1 m^3/s)	(10.1 m^3/s)
Holbox outflow [% of total groundwater outflow	0	54%	0	21%	–	26%	6%
from domain and in m^3/s]	0	(53.9 m^3/s)	0	42.1 m^3/s		51.2 m^3/s	12.5 m^3/s
Total discharge pr. km coast [$m^3/s/km$]	0.20	0.08	0.38	0.30	–	0.27	0.35 (0.95 at the northern coast with diff. K)
SZ max. flow [m^3/s]	−0.6; 0.9	−4; 13	−1; 2	−3; 18	–	−3; 18	−1; 3
x-dir							
y-dir	−1; 0.6	−12; 17	−2; 1	−16; 15	–	−16; 16	−2; 2
OL max. flow [m^3/s]	−0.1; 0.2	−0.2; 0.3	−0.2; 0.2	−0.2; 0.3	–	−0.3; 0.4	−0.2; 0.2
x-dir							
y-dir	−0.2; 0.2	−0.3; 0.3	−0.2; 0.2	−0.3; 0.3	–	−0.4; 0.3	−0.3; 0.2

conduits may become larger and/or have more branches downstream towards the outlet. Therefore, some authors (e.g. Lindgren et al., 2005) assign different K-values along the course of the high-permeability zones. Others (e.g. Kiraly, 2003) use a uniform approach as done here. A third K-value was assigned to the coastal boundary cells in all models (K_{coast}), controlling the coastal leakage. Finally, to take into account the possibility of extensive cave development only in the Pleistocene geology, Conceptual Model 7 was defined. It had a different coastal K-value at the Pleistocene geology (K_{coast_north}) than along the remainder of the coast, and otherwise resembled Conceptual Model 4 with structures and hilly inflow. Conceptual Model characteristics are summarized in Table 1.

Automated inverse calibration was carried out using the nonlinear least squares fitting procedure 'nlinfit' in Matlab (version R2008b, The MathWorks), which uses the Gauss–Newton algorithm with Levenberg–Marquardt modifications. In certain cases the 'robust' fitting option was applied as it gave lower mean square error (MSE) (only used in the calibration of Conceptual Models 5 and 6). Heads in the entire model domain were constrained to be >0 mamsl.

In order to ensure computational efficiency in the calibration a simplified overland flow representation was used. The head in the overland flow cell was set equal to the head in the underlying groundwater cell, and lateral flow in the overland compartment was neglected. Given the high friction in the SKBR overland flow compartment, this approximation is realistic. After model calibration, the overland flow component was enabled and models run again to generate results that included the quantification of overland flow. Due to limited field data, extensive model validation could not be carried out. Instead, the modelled fluxes were compared with literature values to accept or reject the different conceptual models.

Only Conceptual Models 4 and 7 were run in transient mode over a period of five years (2004–2008; the period for which estimates of both monthly precipitation and monthly ET_a were available). The available data was insufficient to calibrate a transient model independently, so K-values from the corresponding steady state model were used. Input was monthly recharge values from Gondwe et al. (2010b). The specific yield (S_y) was adjusted by fitting a modelled transient hydrograph with a measured hydrograph at Dzula. Hilly inflow time series calculated from the recharge data were routed using a linear reservoir model. Time lag was adjusted by comparing with the Dzula hydrograph. A rough comparison with interferograms from Gondwe et al. (2010a) was carried out to investigate the ability of the transient model to produce surface water level changes similar to those observed. For the sensor used in this study, a phase cycle (="fringe") of 0–2π corresponds to 3.9 cm relative water level change. Further details are given in Gondwe et al. (2010a).

2.4. Stochastic catchment simulation

To delineate the catchment of Sian Ka'an, stochastic simulations were carried out with particle tracking. Similar approaches have been used by Vassolo et al. (1998), Stauffer et al. (2002, 2005) and Hendricks Franssen et al., 2004.

Following the inverse calibration, the resulting covariance matrix was used to determine the 95% confidence interval of the calibrated parameters and their cross-correlation. Due to very wide or undetermined 95% confidence intervals for K_{matrix} and K_{struct} when K_{coast} (and K_{coast_north}) was included in the inverse calibration, it was decided to fix K_{coast} (and K_{coast_north}) at the optimal value. The parameters K_{matrix} and K_{struct} were subsequently recalibrated and narrower 95% confidence intervals were obtained. These were used in Monte Carlo catchment simulations. Since K_{coast} varied by less than an order of magnitude in its 95% confidence interval, this approach was considered acceptable. A strong negative cross-correlation between K_{matrix} and K_{struct} existed in the models, where both parameters were calibrated (e.g. Pearson's r was −0.88 (Conceptual Model 2), −0.92 (Conceptual Model 4), −0.86 (Conceptual Model 6)), except in Conceptual Model 7, where this correlation was positive ($r = 0.96$). These cross-correlations were incorporated into the Monte Carlo sampling. The Metropolis–Hastings algorithm (Hastings, 1970) of Matlab ('mhsample') was used. It is a Markov chain Monte Carlo method. The log-K values were sampled in the log-space, and subsequently transformed to their actual values. A multivariate normal distribution was used as probability density function for the log-K values, and random values were drawn using Cholesky decomposition and the Box-Muller transform.

For each equally likely set of K-values, the model was run, and particle tracking using MIKE SHE's random walk Particle Tracking module was applied. Since the effective porosity (φ_{eff}) is unknown, we first determined the steady state catchment, which is independent of φ_{eff}. This (worst case) greater envelope of the catchment was obtained by placing particles at the bottom of the model grid cells in the steady state models and tracking those that ultimately entered the official boundaries of Sian Ka'an. The combined area, where the particles originated from corresponds to the inner and outer protection zones usually used within well protection strategies (e.g. Chave et al., 2006; Milanović, 2004). Probability maps of catchments were then calculated by stacking the results of the realizations. Also groundwater travel time zones are frequently used for groundwater protection and land use zonation, but these results depend strongly on the value of φ_{eff}. Following the recommendations of Worthington and Ford (2009), the travel time zones were delineated in different scenarios by adjusting φ_{eff} so that modelled velocities matched measured groundwater velocities in matrix and caves. Scenario 1 assumed a matrix velocity of 1×10^{-5} m/s and, if the structures were differentiated, a structure (conduit) velocity of 0.03 m/s. Maximum φ_{eff} was set to 0.3 (higher-end value measured by Gonzalez-Herrera, 1984), yielding velocities in the range of 10^{-5} m/s. Scenario 2 assumed a structure velocity of 0.03 m/s and also a matrix velocity of 0.03 m/s. The matrix velocity of 0.03 m/s is relevant if conduits are assumed present in every single 1 km^2 matrix grid cell. This first-order approach of adjusting φ_{eff} values to obtain measured groundwater velocities can be useful to obtain an estimate of first breakthrough times for a water-borne pollution when using equivalent porous medium models. However, it is important to realize that this approach only simulates the fast flow through conduits and fractures. The slow extended release of contaminants from matrix, resulting from conduit-matrix exchange processes, cannot be estimated with this approach, and instead requires more refined transport simulation (Li et al., 2008; Geyer et al., 2007; Spiessl et al., 2007).

For the Conceptual Models 4, 6, and 7, 800 realizations yielded stable probability maps of the catchments. For Conceptual Model 3, only 500 realizations were needed.

3. Results

3.1. Results of Multiple Model Simulation: acceptance and rejection of conceptual models

Calibration results and key model outputs for the different conceptual models are shown in Table 1. All models were calibrated assuming that the equivalent porous medium approach can appropriately simulate regional groundwater flow in the domain. It should be kept in mind that this type of model captures some, but far from all, of the duality of karst aquifers. For steady state solutions, the lack of representing the duality of infiltration is not

a problem. The grid resolution is insufficient to simulate the duality of discharge (through matrix and springs, respectively). Moreover, validation of simulated spring flows is impossible because of lack of in situ observations.

For the models with a uniform coastal leakage, the MSE showed that including structures gave better fits (cf. Conceptual Model 1 and 2; 3 and 4/5/6). Including inflow from the Cretaceous area to the model domain improved model fits as well (cf. Model 1 and 3; 2 and 4). The 100% hilly inflow can apparently be estimated reliably with the surface water catchment method, as calibration of the hilly inflow (Model 5) resulted in almost the same value as Model 4 (105% instead of 100% and same MSE to the 3rd decimal). In these first six Conceptual Models, K_{struct} was always calibrated to be greater than K_{matrix} by 1–2 orders of magnitude. K_{struct} had the same order of magnitude as that used by Kiraly (2003), who used a similar equivalent porous medium modelling method, and determined K_{struct} to be $\geqslant$10 m/s. The calibrated value of K_{coast} was roughly one order of magnitude less than K_{matrix}. Scatter plots of measured vs. modelled heads are shown in Fig. 6. In Conceptual Model 1 the low heads (<1 mamsl) were all modelled 0.5–1 m higher than measured (Fig. 6a). Spatially, these points were located from the northern part of the Sian Ka'an Biosphere Reserve up to the model boundary north of Tulum, in the area around the Holbox fracture zone. Conceptual Model 1 was rejected because of this large low-head discrepancy and the relatively large MSE. The remaining models showed the same overall shape of the scatter plots, which were not appreciably different from one another. Moreover, the MSE of the remaining models were similar. Conceptual Model 7 had the smallest MSE. Conceptual Model 3 showed a similar, but less pronounced spatial bias of residuals in the northern part of the model area around the Holbox zone, as Model 1.

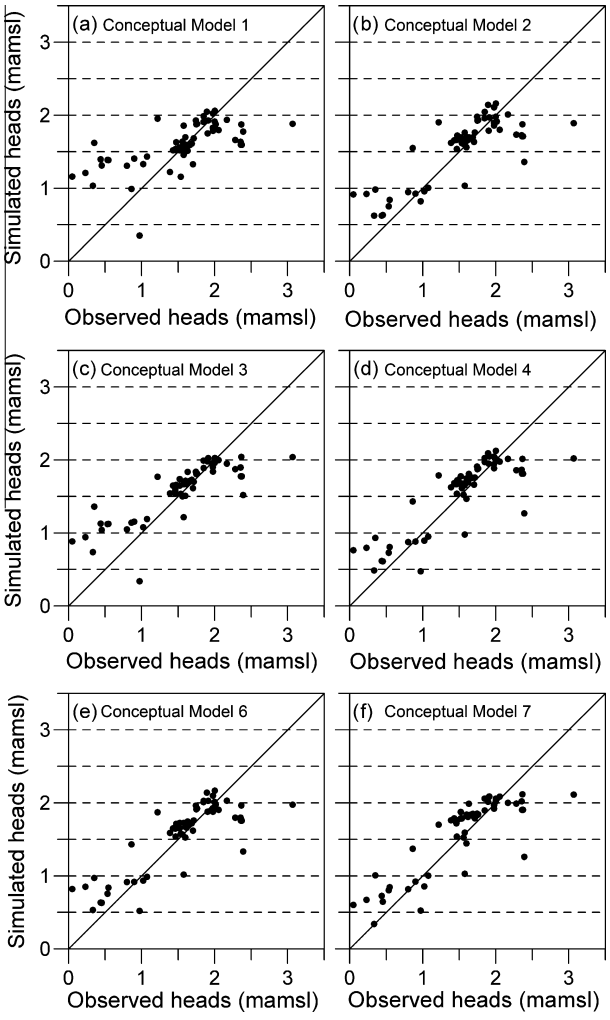

Fig. 6. Measured vs. modelled heads for Conceptual Models 1–4, 6 and 7.

Clearly, the heads in the north near the Holbox zone were the reason why structures were assigned higher K than the matrix, in the models, where structures were included. Conceptual Model 7 showed that when a different K at the coast was allowed in this northern area, coastal leakage was one order of magnitude larger in this area than in the remainder of the model area ($K_{coast\_north} \gg K_{coast}$, Table 1). Because this changed leakage at the coast reduced the modelled heads around the Holbox zone to acceptable levels in Model 7, K_{struct} was not modelled to be appreciably different from K_{matrix} (also seen from their strong positive correlation). When including the overland flow component in the calibrated models, the MSE followed the same pattern as in the models without overland flow, and the MSE improved slightly, except in Models 2 and 6.

Where possible, the model results were compared with values from the literature to clarify whether all the remaining models could be considered plausible. The total discharge per km of coastline was seen to be rather constant in all models, approximately 0.2–0.4 m^3/s/km, except in Conceptual Model 2, which had a low value of 0.08 m^3/s/km. Estimates in the literature range from 0.27 m^3/s/km to 0.73 m^3/s/km (Table 2). In this light the low estimate of Conceptual Model 2 is clearly unrealistic. Therefore, this model was also rejected. The reason for the low coastal outflow in this model was that a large fraction of the total water input exited through the Holbox fracture zone instead (53.9 m^3/s compared to ~120 m^3/s recharge in this model).

The calculated maximum conduit flows were 3–18 m^3/s, when attributing all flow in structure cells to conduit flow, in Models 2, 4, 5, and 6. These values are not unrealistic judging from values reported in the literature (range: 1–17 m^3/s, Table 2). Literature values for overland flow are not available. However, there was little difference between the different model estimates. A rough recalculation to average velocities, using simulated overland water depth and grid cell area, yielded maximum overland flow velocities of 0.3 cm/s, and mean average velocities of 0.007 cm/s. The Shark River Slough of the Everglades also has low hydraulic gradients (3–4.7 cm/km, Bazante et al., 2006) and appears similar to Sian Ka'an's wetlands. Sian Ka'an's modelled overland flow velocities are in the same range as the velocities measured in Shark River Slough (average: 1–1.5 cm/s; range: 0.8–4 cm/s, Bazante et al., 2006). However, the model values represent average velocities for 1 km^2 grid cells, whereas actual velocities are highly determined by local cross-sections, etc.

K_{coast} was calibrated to be in the order of 10^{-2} m/s – one order of magnitude less than K_{matrix} in Conceptual Model 3, 4, and 6. This was in agreement with divers' observations of possible coastal restriction to flow (at least near Tulum), and the same conclusion derived from the freshwater lens thickness > 0 m at the coast. However, the calculated Holbox outflow was very large in these models. In Conceptual Model 7, the calculated Holbox outflow seemed at a more reasonable level, although no field observations on Holbox outflow are available. Yet, in Model 7 K_{coast_north} was not sufficiently low to give the observed freshwater thickness at coast of at least 4.6 m, when using Dupuit–Ghyben–Herzberg computations. The remaining output parameters in Table 1 are not known in reality from other studies. Therefore, there were no reasons to discard the remaining models. Conceptual Models 3, 4, 6, and 7 were all deemed plausible and used in the further analysis. Of these, Models 4 and 7 had the best fits to measured heads.

Fig. 7a shows the modelled depth to groundwater plotted against the mean actual evapotranspiration (average of years 2004–2008) at each grid cell. Standard deviations are given as error

Table 2
Available literature values for model outputs.

Parameter	Value	Reference and comments
Total discharge pr. km coast	0.27 $m^3/s/km$	Hanshaw and Back (1980), NW Yucatan
	0.38 $m^3/s/km$	Thomas (1999), based on total freshwater conduit outflow
	0.73 $m^3/s/km$	Beddows (2004), "crude assumption" from "19 known outflows/80 km of 1 m^3/s each" (i.e. 0.24 $m^3/s/km$) + (her guesstimate to represent further outflow from matrix) 0.5 $m^3/s/km$
SZ max. flow	At cave outlets (submarine springs):	At cave outlets (submarine springs):
	2.43 m^3/s	Back et al. (1979) (measured at Xel Ha)
	1.9 m^3/s	Thomas (1999) (measured at Xel Ha)
	5–9 m^3/s	Beddows (2004) (measured at Xel Ha)
	1.1 m^3/s	Thomas (1999) (measured at Casa Cenote and Abejas)
	2.96 m^3/s	Beddows (2004) (measured at Casa Cenote)
	2.7 m^3/s	Thomas (1999) (measured at Xpu-Ha)
	5.1 m^3/s	Thomas (1999) (measured at Chuchuen, north of model area)
	17 m^3/s	Thomas (1999) (measured at Conil, outlet at north Holbox fracture zone)
	Inside caves:	Inside caves:
	0.8–1.5 m^3/s	Beddows (2003) (estimated from measured dye tracing velocities and conduit dimensions at Nohoch Nah Chich)
	1–13 m^3/s	Neuman and Rahbek (2007) (estimated from pers. comm.. with cave divers)
Groundwater flow velocity	At/near cave outlets:	At cave outlets:
	0.012 m/s	Moore et al. (1992) (measured)
	0.055 m/s	Beddows (2004) (measured, Casa Cenote, average value)
	0.3 m/s	Beddows (2004) (measured, Casa Cenote and Xel Ha, maximum values)
	1 m/s	Estimate from divers' scooter, Sistema Manatee (cave diver Le Maillot, pers. comm. in Neuman and Rahbek, 2007)
	Inside caves:	Inside caves:
	0.001 m/s	Moore et al. (1992) (measured)
	0.006 m/s	Beddows (2003) (from dye tracing, lowest for dye peak)
	0.030 m/s	Beddows (2003) (from dye tracing, largest for dye peak)
	0.009 m/s	Beddows (2003) (from dye tracing, lowest for dye front)
	0.075 m/s	Beddows (2003) (from dye tracing, largest for dye front)
	0.023 m/s	Beddows (2004) (from dye tracing, average value Heaven's Gate)
	0.014 m/s	Beddows (2004) (from dye tracing, average value River Run/Ponderosa)
	In matrix:	In matrix:
	2.1e−4 m/s	Moore et al. (1992) (measured in a borehole several km from coast; considered upper range velocity estimate)
	4.6e−7 m/s	Neuman and Rahbek (2007) (estimate from numerical conduit-matrix modelling, considered lower range velocity estimate)

bars. Also reference evapotranspiration, calculated with Hargreaves' equation (see Gondwe et al., 2010b) is shown (average of years 2004–2008). At sites with depth to groundwater between 0 and about 8 m below ground (mbg) evapotranspiration took place at the potential rate ($ET_a = ET_{ref}$). At sites with depth to groundwater between 30 and 50 mbg, ET_a was constant, and hence did not depend on the depth to groundwater. The vegetation was also equally dense and equally structured here (constant Vegetation Index (EVI from MODIS), Fig. 7b), and vegetation maps show uniform vegetation (INEGI, 1997). However, at sites with depth to groundwater between about 8–10 m and 30 m, a decreasing ET_a-rate with increasing depth to groundwater could be observed. The relationship was linear ($R^2 = 0.87$). A decrease in ET_{ref} at these sites was clearly not part of the explanation. On the contrary, ET_{ref} was seen to increase in this interval. Differences in vegetation also did not appear to be the explanation, as EVI was rather constant here (Fig. 7b) and vegetation maps did not reveal any differences.

3.2. Scenarios to assess impact of recharge and Holbox boundary uncertainty

Scenario analyses (Tables 3 and 4) were carried out on the two models giving the smallest MSE, namely Conceptual Model 4 and 7. The scenario analyses focused on two parameters: the Holbox fixed head boundary and the recharge. These parameters were kept fixed in the previous calibrations, but since these inputs are uncertain, the effect of these uncertainties needed to be assessed.

When varying the Holbox fixed head boundary by ±4 cm, the model structure of Model 4 was robust (K_{struct} always $\gg K_{matrix}$), whereas the model structure of Model 7 was not robust (K_{coast_north} became $\geqslant K_{matrix}$, whereas it was $< K_{matrix}$ originally. K_{struct} became $< K_{matrix}$, whereas the two had been practically equal originally). Resulting outflows through the Holbox zone, however, remained at the same magnitudes as in the original models.

Also in the scenarios with changed recharge, the model structure of Model 7 was not robust (Table 4). The model structure of Model 4 remained robust despite the parameter change ($K_{struct} > K_{matrix}$). Outflow from the saturated zone was sensitive to a change in the recharge in both models, since this affected the water balance directly. The Holbox outflow was also very sensitive to changes in recharge. All Holbox outflows were reduced, either due to the change in calibrated K_{struct} (when recharge was increased) or due to reduced water input (recharge) to the model. In Model 4, maximum groundwater flow rates ('SZ max. flow') were sensitive to recharge changes, since flow rates were influenced by the resulting changes in K_{struct}.

3.3. Probability maps of catchments

The resulting probability maps for the steady state catchments from Conceptual Models 3, 4, 6, and 7 are seen in Fig. 8. The steady state catchments encompassed roughly the same area west of Sian Ka'an, and had the same east–west maximum extent. There were however also important differences, especially in the south-central

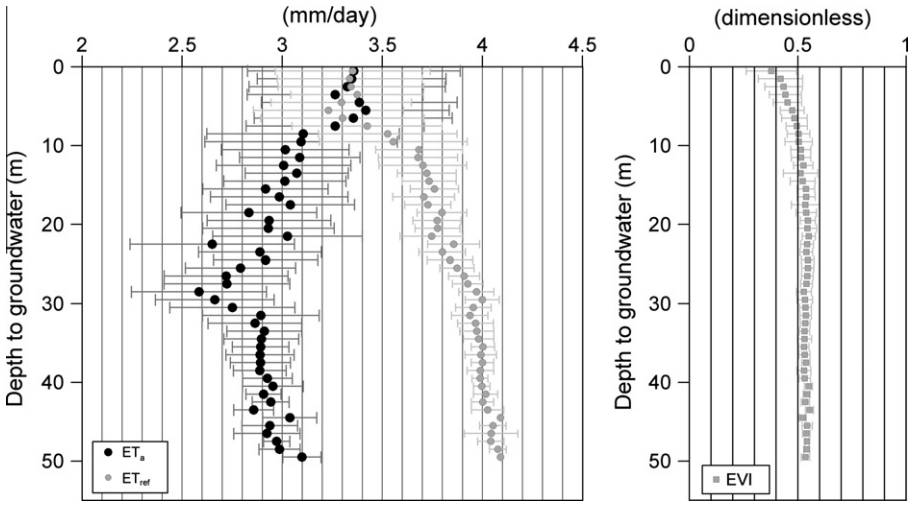

Fig. 7. Actual (ET_a) and reference (ET_{ref}) evapotranspiration, as well as Enhanced Vegetation Index from MODIS (EVI), plotted against modelled depth to groundwater.

Table 3
Results of sensitivity analysis to changes in the Holbox fixed head boundary for Conceptual Models 4 and 7.

Model	$+\sigma_{Holbox\_bound}$ (Model 4)	$-\sigma_{Holbox\_bound}$ (Model 4)	$+\sigma_{Holbox\_bound}$ (Model 7)	$-\sigma_{Holbox\_bound}$ (Model 7)
MSE [m^2]	0.1179	0.1149	0.1027	0.1015
K_{coast} [m/s]	0.058	0.061	0.083	0.091
$K_{coast,\_north}$ [m/s]	–	–	1.87	0.92
K_{matrix} [m/s]	0.61	0.63	0.96	0.86
$K_{structs}$ [m/s]	20.59	14.93	0.62	0.79
MSE with OL [m^2]	0.1180	0.1141	0.1068	0.1032
Holbox outflow [m^3/s]	42.5 m^3/s (change: +0.4 m^3/s or +1%)	39.3 m^3/s (change: −2.7 m^3/s or −7%)	8.9 m^3/s (change: −3.6 m^3/s or −29%)	10.7 m^3/s (change: −1.7 m^3/s or −14%)

Table 4
Results of recharge sensitivity analysis for Conceptual Models 4 and 7.

Model	$+\sigma_R$ (Model 4)	$-\sigma_R$ (Model 4)	$+\sigma_R$ (Model 7)	$-\sigma_R$ (Model 7)
MSE [m^2]	0.1136	0.1213	0.1008	0.1043
K_{coast} [m/s]	0.10	0.05	0.14	0.06
$K_{coast,\_north}$ [m/s]	–	–	1.38	0.92
K_{matrix} [m/s]	0.71	0.65	1.04	0.81
$K_{structs}$ [m/s]	5.31	12.63	0.44	1.11
MSE with OL [m^2]	0.1115	0.1126	0.1033	0.1077
$\frac{OL\_Outflow\_all\_domain}{SZ\_Outflow\_all\_domain}$ [% and OL outflow in m^3/s]	6.5% (13.6 m^3/s)	12.4% (18.0 m^3/s)	4.2% (9.4 m^3/s)	7.5% (13.3 m^3/s)
$\frac{SZ\_Outflow\_SKBR}{SZ\_Outflow\_all\_domain}$ [% and SKBR SZ outflow in m^3/s]	44.8% (92.1 m^3/s)	46.2% (67.4 m^3/s)	44.7% (99.5 m^3/s)	42.7% (75.1 m^3/s)
$\frac{OL\_Outflow\_SKBR}{SZ+OL\_Outflow\_all\_domain}$ [%]	4.6%	8.6%	3.1%	5.1%
Within SKBR only: $\frac{OL\_Outflow}{SZ\_Outflow}$ [% and SKBR OL in m^3/s]	10.3% (9.5 m^3/s)	8.6% (12.5 m^3/s)	6.9% (6.8 m^3/s)	11.9% (8.9 m^3/s)
Holbox outflow [m^3/s]	23.9 (change: −18 m^3/s; −43%)	35.3 (change: −7 m^3/s; −16%)	10.5 (change: −2 m^3/s; −16%)	9.6 (change: −3 m^3/s; −23%)
Total discharge pr. km coast [m^3/s/km]	0.38	0.27	0.41 (at north coast: 1.03)	0.32 (at north coast: 0.85)
SZ max. flow [m^3/s]	−1.3; 7.2	−1.9; 12.3	−1.0; 4.1	−0.9; 2.4
x-dir				
y-dir	−4.5; 6.1	−9.6; 10.3	−2.5; 2.4	−1.8; 1.3
OL max. flow [m^3/s]	−0.2; 0.2	−0.3; 0.3	−0.2; 0.2	−0.2; 0.2
x-dir				
y-dir	−0.2; 0.2	−0.3; 0.3	−0.2; 0.1	−0.3; −0.2

part of the model area, where structures were prevalent. In Model 3, the shape of the steady state catchment was stable under parameter changes. The probability that a particular model cell was part of the steady state catchment was either 0 or 1. In the other models, the shape of the steady state catchment was variable and probabilities ranged from 0 to 1. This was due to the different combinations of K_{struct} and K_{matrix} values in each realization. Conceptual Model 4 had the most extensive catchment area when considering all probabilities >0. This steady state catchment and that of Model 6 were clearly influenced by the higher-permeable structures. Model 7's steady state catchment was influenced by the inflow from the hilly area, and thus bended slightly towards the south further inland. In Models 4, 6, and 7 the steady state catchments in reality also include an unknown part of the hilly area.

The estimated values of φ_{eff} ranged above or within the interval 1×10^{-4}–1×10^{-3}, which Worthington and Ford (2009) suggested

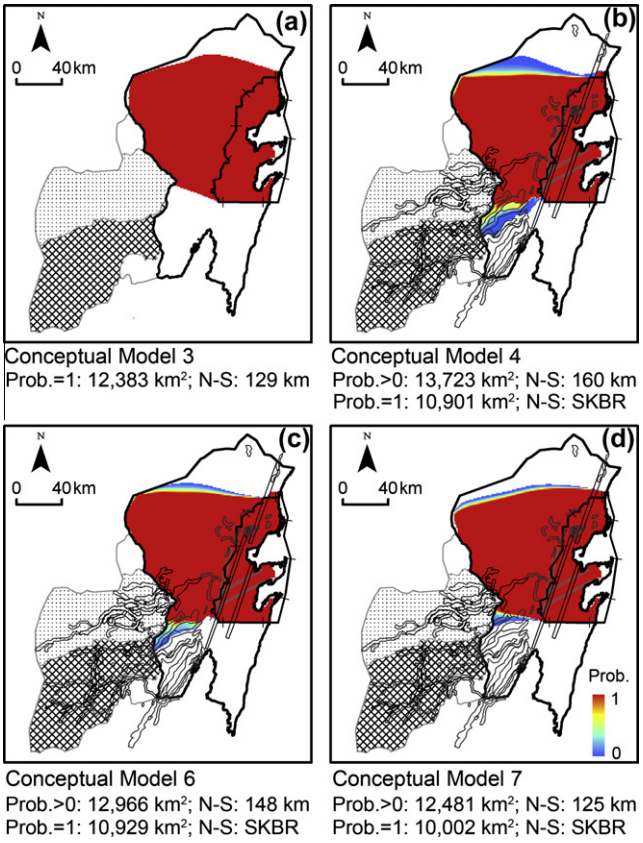

Fig. 8. Probability (Prob.) of a cell belonging to Sian Ka'an's steady state catchment, for Conceptual Models 3, 4, 6 and 7.

to use in equivalent porous medium models for transport simulations that should imitate the rapid transport through conduits. Only when the average matrix velocity of Model 4 was equal to 0.03 m/s, a lower φ_{eff} of 3×10^{-5} was estimated. Zones of travel times to the boundary of Sian Ka'an are shown in Fig. 9, for different velocities and different scenarios. The 0–24 h, 1–10 day and 11–50 day travel time zones correspond to the protection zones II and III of Milanović (2004) (zone III may extend to either 10 days or 50 days travel time). The 0.13–1 year, 2–10 year and 11–20 year protection zones are used by some countries as inner, middle, and outer protection zones, but not specifically within karst (Chave et al., 2006).

3.4. Transient dynamics

The specific yield and the lag time of the hilly inflow was obtained from comparing measured and modelled heads at Dzula, and gave $S_y = 0.4$ and a lag time of about 3 months (Fig. 10). The lag time of 3 months corresponded well with a correlation between Sian Ka'an's flooding dynamics and a 3-months backward moving average of catchment precipitation (Gondwe et al., 2010a).

Fits were satisfactory when comparing measured and modelled heads at all 59 wells at the four points in time, where measurements were available. Median difference between measured and modelled heads was 3–14 cm for Model 4 and 1–8 cm for Model 7. Scatter plots showed no notable difference between the fits of the two models to measured heads at different times.

The modelled flooding dynamics showed most water in the Sian Ka'an wetlands in the months December–January, and least water in April to August, for both Model 4 and Model 7. This corresponds fairly well with radar-derived flooding results from August 2006 to

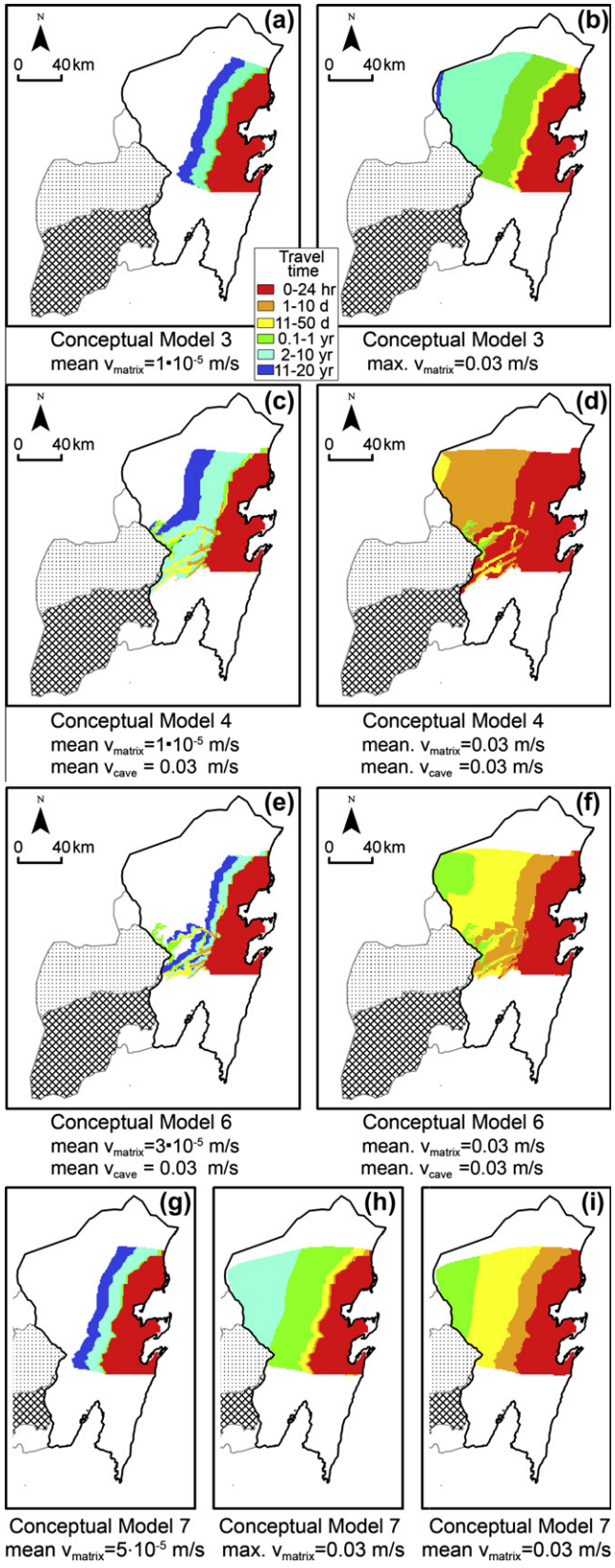

Fig. 9. Modelled travel time zones for different conceptual models and different values of φ_{eff}, adjusted to give the indicated modelled water travel times (v).

February 2008. They showed maximum flooding in December in normal years and minimum flooding in May (Gondwe et al., 2010a). The modelled flooding extent within SKBR varied little in

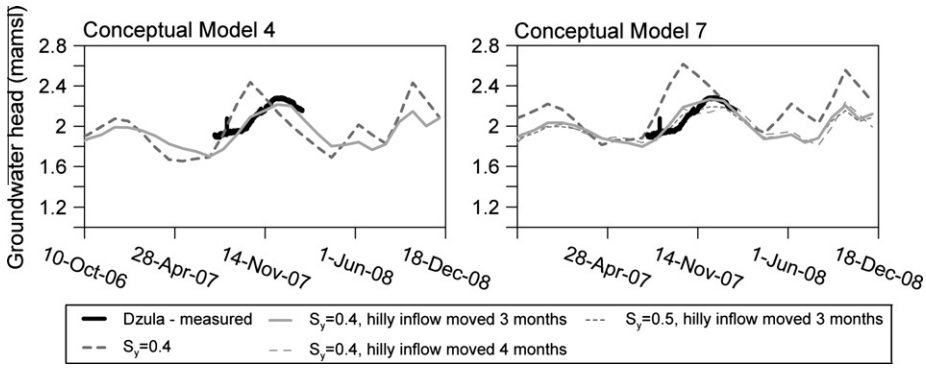

Fig. 10. Measured and modelled Dzula hydrograph, with different values of S_y and lag times for the hilly inflow.

time (from 1750 to 1830 km^2 flooded area). This is because the topographic distribution of values in the SRTM dataset does not reflect the actual bathymetry of the wetlands. Therefore, the transient models could not be calibrated with the flooding extent time series of Gondwe et al. (2010a). However, the modelled flooding extent was in the same range as that observed in the flooding maps of Gondwe et al. (2010a) within SKBR's boundary (mean: 1730 km^2; minimum: 1110 km^2; maximum: 2090 km^2).

Lack of bathymetric data, lack of micro-topographic data, and the large grid-size used in the numerical models hampered comparison of the model results with measured water level changes from interferograms in Gondwe et al. (2010a). However, overall the numerical models tended to have the same overall fringe directions as the observed interferograms, which indicates that the overall pattern of water level changes resembled reality fairly well. The simulated fringe directions in the Chunyaché slough, the Tigritos slough, and the Santa Rosa slough were close to those observed (Fig. 11b and c). The observed north–south fringe direction in the Espíritu slough was not captured in the numerical models, but was likely due to micro-topographic effects (Gondwe et al., 2010a), which were not captured by the topographic data used in the model. Like the observed interferograms, the modelled interferograms generally had few fringes (up to e.g. 5); thus, the modelled relative surface water level changes were rather small, as they are in reality (Gondwe et al., 2010a). Between the two conceptual models there were differences in timing of interferogram changes, but it was not possible to clearly distinguish whether one model was superior to the other. An example of a modelled and an observed interferogram from the same time period is shown in Fig. 11a and b.

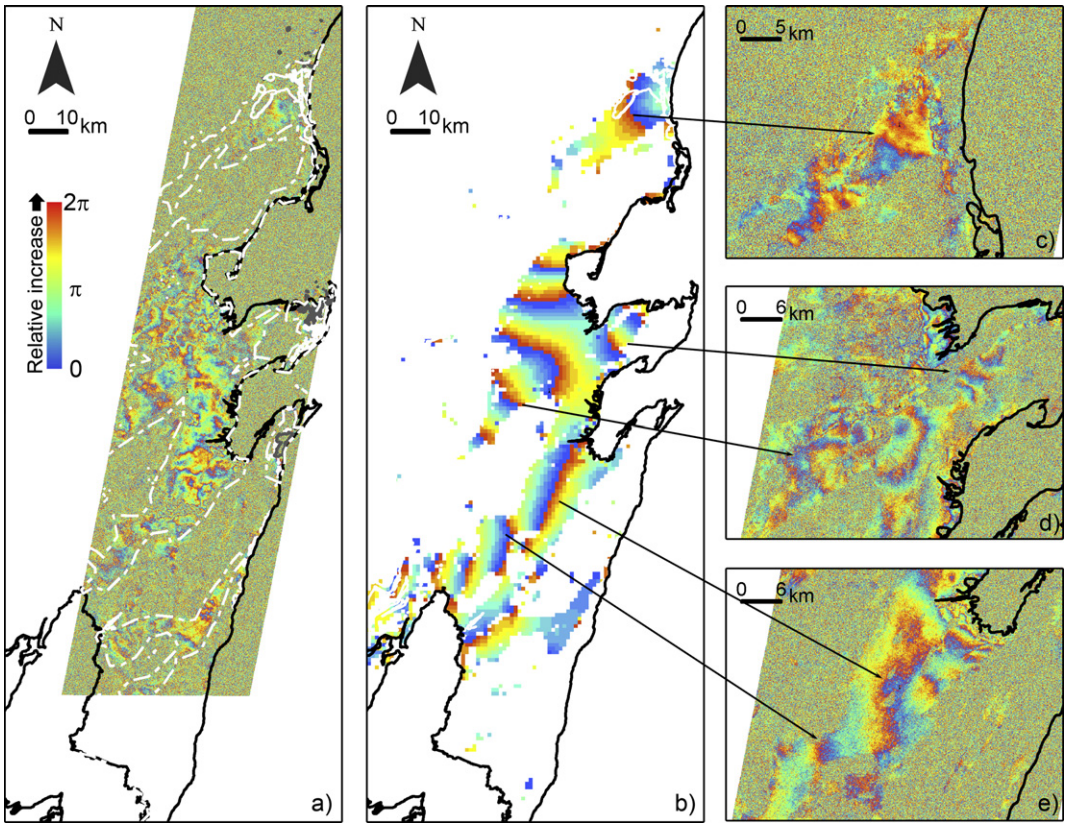

Fig. 11. Observed (a) and modelled (b) interferogram for October–December 2007, and observed interferogram examples from other dates showing characteristic fringes of the interferograms which are also found in the modelled interferogram (c–e). Modelled example was generated by Conceptual Model 4. Legend shows relative water level increase or decrease. (c) Chunyaché slough, June–August 2007. (d) Tigritos and Santa Rosa slough June–August 2007. (e) Espíritu slough, November–December 2006.

4. Discussion

4.1. The impact of conceptual model uncertainty on management decision making

The steady state catchments (Fig. 8) show that conceptual model uncertainty affects the extent of the steady state catchment. The nature of the structures determines whether the south-central area of the model domain and Cretaceous area contribute water to SKBR. In these areas agricultural activities are presently expanding, which will possibly lead to increased use of pesticides and fertilizers.

Given the limited field data availability, it is impossible to decide between the different conceptual models. However, methods exist for combining the results from multiple conceptual models: pooling (linear combination of the results with equal weights assigned to each model, Block et al., 2009 and references herein), linear regression weighting (linear combination of results, weights of each model determined from regression coefficient of observed vs. modelled conditions for each model, Block et al., 2009 and references herein), and Bayesian model averaging (e.g. Neuman, 2003; Rojas et al., 2008, 2009; Li and Tsai, 2009). For transient models, the 'hierarchical mixture of experts' framework (Marshall et al., 2006) and kernel density estimators (Block et al., 2009) may be used to let the weight of each model in a linear combination vary in time. Moreover, non-linear weighting of conceptual models by means of artificial neural networks has been applied (Xiong et al., 2001). Combining different conceptual models typically provides more robust results than using one single conceptual model (e.g. Georgakakos et al., 2004; Rojas et al., 2008; Block et al., 2009). Combinations may, however, be sensitive to the assumptions used in the analysis. For instance, Rojas et al. (2009) showed that Bayesian averaging methods rely not only on the posterior probabilities of each model (i.e. the weights used), but also on the prior model probabilities, i.e. the assumed probability distributions of the model input parameters.

The travel time zones in Fig. 9 show the significant influence of the choice of conceptual model, as well as φ_{eff}, on management decisions. Here, the influence of the structures on the areas that need to be protected in some way is even clearer than in the steady state catchments for Models 4 and 6. The various φ_{eff} chosen yield a very large difference in the extent of the protection zones for the models. Because it is impossible and economically unfeasible in practice to provide a high degree of aquifer protection to the whole steady state catchment, the φ_{eff} and/or actual groundwater travel times must be determined more accurately to be able to carry out efficient groundwater protection.

4.2. Discussion of the most robust modelling results

Results from all of the accepted conceptual models showed that groundwater outflow through the coastline within SKBR's boundary is 68–90 m^3/s. The groundwater that passes through Sian Ka'an is therefore a significant contribution to the marine environment, which hosts one of the most productive coral reef systems in the world, but which is also sensitive to changes in water quality (TNC, 2008; Lang et al., 1998). Therefore, it is clear that if the groundwater that flows into Sian Ka'an is protected, also a high water quality for the marine environment outside Sian Ka'an is ensured.

The overland flow within Sian Ka'an's wetlands equals about 4–12% of the total outflow from the model domain – within Sian Ka'an's boundary 7–16% of the outflow. In absolute numbers overland flow is on the order of 7–13 m^3/s. The overland flow is thus non-negligible, and constitutes an important part of the total water resource. However, groundwater flow within Sian Ka'an is much larger than the overland flow. This has to be taken into account when designing water flow and water quality monitoring networks for SKBR.

The hydrological models also show that the Sian Ka'an wetlands only exist due to recharge from the catchment. The wetlands are indeed groundwater-fed. Recharge over Sian Ka'an itself only constitutes, on average, about 41 million m^3/year, whereas the total average outflow from Sian Ka'an, according to the models, is ~2700–2900 million m^3/year, of which ~280–540 million m^3/year exits via the wetlands (overland flow). The timing of the flooding peaks is also different from the timing of the rainfall maximum and further indicates that Sian Ka'an's wetland dynamics is controlled by the catchment.

Main overland outflows within Sian Ka'an took place at Bahía de la Ascensión and Bahía del Espíritu Santo. The average water depth in the wetlands varied from 0.5 to 1 m in the transient model runs, with the maximum varying from 1.2 to 2.5 m. The real water depth may be somewhat different locally, because the model does not take local bathymetry into account. Given the amount of recharge and the high aquifer transmissivities, groundwater abstractions in the catchment are unlikely to have a detrimental effect on the wetlands. Only direct water abstractions from the wetlands themselves could affect the wetlands' water quantities negatively, because the freshwater lens is thinner in this near-coastal zone, and since wetland ecosystems depend on certain hydroperiods, flooding frequencies, flooding areas, and flooding depths (Powell et al., 2008; Acreman and Dunbar, 2004).

From the recharge estimates and the modelling results, the overall water balance of the model domain can be determined. Direct recharge via infiltration constitutes 17 ± 3% of the mean annual precipitation in the model domain (recharge: 4400 million m^3/year ± 700 million m^3/year). Boundary inflows from the hilly area may be of similar magnitude. Water exits the domain through overland flow (4–12%) and groundwater flow (88–96%). The latter is distributed between coastal outflow to the sea, and groundwater outflow towards the north via the Holbox fracture zone. The distribution between these two groundwater sinks is presently uncertain. However, it appears relatively certain that there *is* some water flowing through the Holbox fracture zone from south to north, on average. Groundwater flow through the Holbox is in agreement with the dye tracing results of Beddows and Hendrickson (2008).

The modelled flooding dynamics and the flooding dynamics from Gondwe et al. (2010a) show that the months April–August are probably the most vulnerable times of the wetlands, since any water-borne pollutants may be less diluted at these times and low water amounts may create increased vulnerability to reduction in water quantity. The high flow periods (December–January) and the medium flow periods (in between) are, however, also important to maintain the natural cycle of the wetlands.

It is worth noting the dependence of ET_a on the depth to groundwater in areas, where the groundwater is located 0–30 mbg. This finding has not previously been shown for the Yucatan Peninsula. The only study known to the authors, which investigates water source of the vegetation in the region, has not shown that trees rely on groundwater as a source of water (Querejeta et al., 2007). However, the correlation between ET_a and depth to groundwater seen in Fig. 7 indicates that uptake of groundwater by trees and plants in the model domain does seem to have some importance in the areas, where groundwater is <30 m from the surface. The relation between ET_a and depth to groundwater appears to be represented by a segmented line (Banta, 2000; Luo et al. 2009). In another karstic aquifer, yet not tropical, this has also been observed – roots could reach as deep as 25 mbg, and the deep roots were found specially optimized for deep water uptake (Jackson

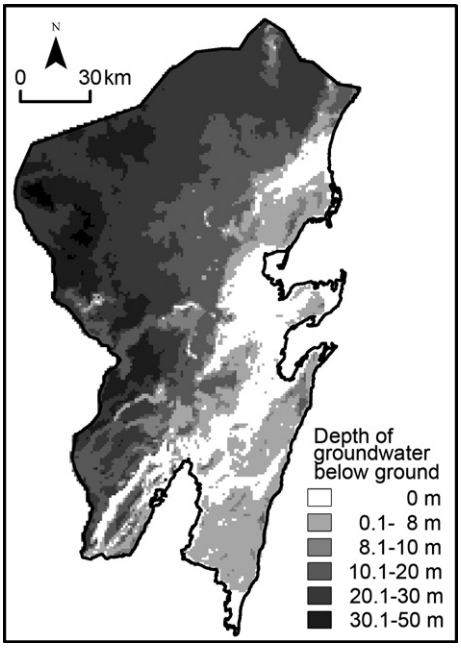

Fig. 12. Modelled depth to groundwater below topographic surface. Areas with groundwater ⩽8 mbg are likely to be groundwater-dependent ecosystems (see text). Areas with groundwater 8–30 mbg may be partially groundwater-dependent (see text). White areas have overland water.

et al., 1999; McElrone et al., 2004; Pockman et al., 2008). The areas with groundwater ⩽8 mbg seem to be groundwater-dependent ecosystems – they have full access to water enabling them to transpire at potential rate. These areas are shown in Fig. 12.

The discharge per km of coast was in all models estimated to be about 0.3–0.4 $m^3/s/km$, which fits well with other estimates. The discharge along the coast near Tulum may or may not be higher than this (~1 $m^3/s/km$). The K_{coast} calibrated as $<K_{matrix}$ (except, perhaps, around Tulum) shows that indeed there appears to be restriction to outflow at the coast. A freshwater lens thickness >0 m at the coast in the whole model domain results from this. For local management purposes this is important to note. The extensive hotel construction taking place along the coast at Riviera Maya, and proposed for the Costa Maya, should ensure that this coastal restriction to outflow is maintained. The coastal freshwater resources are already limited. On a local (plot) scale they may be further reduced if the coastal restriction to outflow is breached, and since hotels often abstract water from their own plot (Beddows, 2002), they should have an interest in maintaining the fresh water lens as thick as possible near the coast.

The K_{matrix} calibrated in the models appears realistic. It is in the same order of magnitude as that estimated from geophysical measurements of depth to the halocline in Gondwe et al. (2010b) (estimated to be 0.6 m/s when recharge constitutes ~400 mm/year, as in the case, where 100% inflow from the hilly area is present).

5. Conclusions

Through automatic calibration and stochastic modelling, probability maps of the steady state catchment for the groundwater-dependent Sian Ka'an wetlands have been calculated. The use of different conceptual models shows that the conceptual model structure will have a huge impact on management decisions for karst aquifers. The same applies for the effective porosity, as it determines the extent of protection zones derived from groundwater travel times. Multiple Model Simulation is a useful way to examine the effect of conceptual uncertainty. Furthermore, through this method and scenarios that vary uncertain model input parameters, directions for further research can be obtained, as these methods reveal the most sensitive concepts and parameters for a management perspective. It is important to further investigate the properties of the structures – specifically whether they conduct water flow more easily than the surrounding matrix. It should also be determined whether coastal leakage is larger near Tulum than elsewhere in the model domain. Tracer testing could be carried out in the catchment to better determine φ_{eff} and the extent of the travel time zones. Inflow from the Cretaceous area may be important. The surface water catchments (Fig. 4) may be an acceptable first-order approach to determine, where the water in the hilly area comes from. However, further studies of the hilly area's hydrogeology are warranted. The models' validity could be further investigated and improved if flow measurements from aquifer and conduits, and hydrograph data from springs, could be obtained in the future. If such data became available, choosing a different numerical representation of the aquifer than the equivalent porous medium, such as a double-continuum representation, could be relevant for this aquifer. Double-continuum models are better and more precise representations of karst aquifers, but not feasible at the scale of this study. However, on a local scale they are highly relevant, and would be nested into a regional groundwater flow model, such as the ones presented in this study.

The spatial outputs from the hydrological models enable land use zonation based on aquifer protection concepts, and enable aquifer vulnerability mapping. Vulnerability mapping is applicable for well-field and ecosystem protection and management, but can also be valuable for guiding urban and tourism development plans in the area. The water balance insights from the hydrological modelling shows the importance of both the overland flows and the groundwater flows within Sian Ka'an, both for Sian Ka'an's ecosystems and for the marine environment, which is the final recipient of the outflows. The hydrological modelling indicates that groundwater may exit the model domain to the north through the Holbox fracture zone. This is important in order to understand the peninsular-scale hydrologic relation between regions.

Acknowledgements

We gratefully acknowledge financial support from the WWF Verdensnaturfonden/Aase & Ejnar Danielsens Fond 2006 and 2007, the COWIfoundation, Amigos de Sian Ka'an and the Technical University of Denmark.

We acknowledge comments and suggestions from three anonymous reviewers, which significantly improved this manuscript.

References

Acreman, M., Dunbar, M.J., 2004. Defining environmental river flow requirements – a review. Hydrol. Earth Syst. Sci. 8 (5), 861–876.

ASK, 2003. Tratamiento de Aguas Residuales. Report prepared by Amigos de Sian Ka'an A.C. (ASK). Available on the cd-rom of the workshop: Construyendo las Bases Para la Conservación del Agua y su Biodiversidad Asociada en la Península de Yucatan". 10 y 11 de noviembre 2003, Cancún Quintana Roo, Organizado por Amigos de Sian Ka'an, The Nature Conservancy y la Comisión de Áreas Naturales Protegidas.

Atkinson, T.C., 1977. Diffuse flow and conduit flow in limestone terrain in the Mendip Hills, Somerset (Great Britain). J. Hydrol. 35, 93–110.

Back, W., Hanshaw, B.B., Pyle, T.E., Plummer, L.N., Weidie, A.E., 1979. Geochemical significance of groundwater discharge and carbonate solution to the formation of Caleta Xel Ha, Quintana Roo, Mexico. Water Resour. Res. 15 (6), 1521–1535.

Banta, E.R., 2000. MODFLOW-2000. The US Geological Survey Modular Ground-Water Model – Documentation of Packages for Simulating Evapotranspiration with a Segmented Function (ETS1) and Drains with Return Flow (DRT1). US Geol. Surv. Open-File Rep. 00-466, pp. 127.

Bauer, S., Liedl, R., Sauter, M., 2003. Modeling of karst aquifer genesis: influence of exchange flow. Water Resour. Res. 39 (10), SBH61–SBH612.

Bazante, J., Jacobi, G., Solo-Gabriele, T., Reed, D., Mitchell-Bruker, S., Childers, D.L., Leonard, L., Ross, M., 2006. Hydrologic measurements and implications for tree

island formation within Everglades National Park. J. Hydrol. 329, 606–619. doi:10.1016/j.jhydrol.2006.03.011.
Beddows, P.A., 2002. Where does the sewage go? The karst groundwater system of Municipalidad Solidaridad, Quintana Roo. Assoc. Mex. Cave Stud. Activ. Newsl. 25, 47–52.
Beddows, P.A., 2003. Cave hydrology of the Caribbean Yucatan coast. Assoc. for Mex. Cave Stud. Bull. 11. Austin, TX, USA.
Beddows, P.A., 2004. Groundwater hydrology of a coastal conduit carbonate aquifer: Caribbean coast of the Yucatán Peninsula, México. PhD thesis. Sch. of Geogr. Sci. Univ. of Bristol, UK.
Beddows, P.A., Hendrickson, M.R., 2008. When the survey is not enough: temperature, salinity, and dye tracing reveal flow paths. In: Elliot, W.R. (Ed.), Proc. 2007 Natl. Cave and Karst Manage. Symp., St. Louis, Mo., USA, pp. 198–203.
Beddows, P.A., Smart, P.L., Smith, S. L., Whitaker, F.F., 2005. Potential for inland dispersal of injection well effluent in coastal carbonate aquifers: evidence from Caribbean Yucatan coast. In: Proc. 2005 Natl. Cave and Karst Manage. Symp., Albany, NY, USA.
Beddows, P.A., Smart, P.L., Whitaker, F.F., Smith, S.L., 2007. Decoupled fresh–saline groundwater circulation of a coastal carbonate aquifer: spatial patterns of temperature and specific electrical conductivity. J. Hydrol. 346, 18–32.
Birk, S., Liedl, R., Sauter, M., Teutsch, G., 2003. Hydraulic boundary conditions as a controlling factor in karst genesis: a numerical modeling study on artesian conduit development in gypsum. Water Resour. Res. 39 (1), SBH21–SBH214.
Block, P., Souza Filho, F.A., Sun, L., Kwon, H.-H., 2009. A streamflow forecasting framework using multiple climate and hydrological models. J. Am. Water Res. Assoc. 45 (4), 828–843. doi:10.111/j.1752-1688.2009.00327.
Charvet, G., 2009. Exploration, modeling and management of groundwater resources in Northern Quintana Roo, Mexico. Master thesis. Dept. of Environ. Eng., Tech. Univ. of Den., Kgs. Lyngby, Den.
Chave, P., Howard, G., Schijven, J., Appleyard, S., Fladerer, F., Schimon, W., 2006. Groundwater protection zones. In: Schmoll, O., Howard, J., Chilton, J., Chorus, I. (Eds.), Protecting Groundwater for Health – Managing the Quality of Drinking-Water, WHO. IWA Publ., pp. 465–492 (Chapter 17, ISBN:92-4-154668-9).
Cheng, J.M., Chen, C.X., 2005. An integrated linear/non-linear flow model for the conduit-fissure-pore media in the karst triple void aquifer system. Environ. Geol. 47, 163–174. doi:10.1007/s00254-004-1128-7.
Durlofsky, L.J., 1992. Representation of grid block permeability in course scale models of randomly heterogeneous porous media. Water Resour. Res. 28 (7), 1791–1800.
Eamus, D., Froend, R., 2006. Groundwater-dependent ecosystems: the where, what and why of GDEs. Aust. J. Bot. 54, 91–96.
Escolero, O.A., Marín, L.E., Steinich, B., Pacheco, J., 2000. Delimitation of a hydrogeological reserve for a city within a karstic aquifer: the Merida, Yucatan example. Landsc. Urban Plan. 51, 53–62.
Fideicomiso Para la Promoción Turística de la Rivera Maya, 2004. Estadísticas de Riviera Maya.
Georgakakos, K., Seo, D.-J., Gupta, H., Shaake, J., Butts, M.B., 2004. Towards the characterization of streamflow simulation uncertainty through multimodel ensembles. J. Hydrol. 298, 222–241. doi:10.1016/j.jhydrol.204.03.037.
Geyer, T., Birk, S., Licha, T., Liedl, R., Sauter, M., 2007. Multitracer test approach to characterize reactive transport in karst aquifers. Ground Water 45 (1), 36–45. doi:10.1111/j.1745-6584.2006.00261.
Gondwe, B.R.N., Hong, S.-H., Wdowinski, S., Bauer-Gottwein, P., 2010a. Hydrologic dynamics of the ground-water-dependent Sian Ka'an wetlands, Mexico, derived from InSAR and SAR data. Wetlands 30, 1–13. doi:10.1007/s13157-009-0016-.
Gondwe, B.R.N., Lerer, S., Stisen, S., Marín, L., Rebolledo-Vieyra, M., Merediz-Alonso, G., Bauer-Gottwein, P., 2010b. Hydrogeology of the south-eastern Yucatan Peninsula: new insights from water level measurements, geochemistry, geophysics and remote sensing. J. Hydrol. 389, 1–17. doi:10.1016/j.jhydrol.2010.04.044.
Gondwe, B.R.N., Ottowitz, D., Supper, R., Merediz Alonzo, G., Bauer-Gottwein, P., (submitted for publication). Regional-scale airborne electromagnetic surveying of the Yucatan karst aquifer: geological and hydrogeological interpretation. Hydrogeol. J.
Gonzalez-Herrera, R.A., 1984. Correlacion de Muestras de roca en Pozos de la Ciudad de Merida. Civil engineering thesis. Facultad de Ingeneria, Universidad de Yucatan, Merida, Yucatan, Mexico, pp. 129.
Graham, D.N., Butts, M.B., 2006. Flexible integrated watershed modeling with MIKE SHE. In: Singh, V.P., Frevert, D.K. (Eds.), Watershed Models. CRC Press, pp. 245–269 (Chapter 10, ISBN:0-8493-3609-0).
Hanshaw, B.B., Back, W., 1980. Chemical mass-wasting of the northern Yucatan Peninsula by groundwater dissolution. Geological 8, 222–224.
Hastings, W.K., 1970. Monte Carlo sampling methods using Markov chains and their applications. Biometrika 57 (1), 97–109.
Hendricks Franssen, H.-J., Stauffer, F., Kinzelbach, W., 2004. Joint estimation of transmissivities and recharges – application: stochastic characterization of well capture zones. J. Hydrol. 294, 87–102. doi:10.1016/j.jhydrol.2003.10.021.
Hill, M.C., 1990. Preconditioned Conjugate-Gradient 2 (PCG2), a Computer Program for Solving Ground-Water Flow Equations. US Geol. Surv. Water Res. Investig. Report 90-4048. Second Printing, 2003.
Højberg, A.L., Refsgaard, J.C., 2005. Model uncertainty – parameter uncertainty versus conceptual models. Water Sci. Technol. 52 (6), 177–186.
INEGI, 1997. Carta de uso de suelo y vegatación (vegetation map). Recursos electónicos. Escala 1:250,000. Instituto Nacional de Estadística Geogrfía e Informática (INEGI). Shape file.
ITC, 2005. ILWIS 3.3 Academic. International Institute for Geo-Information Science and Earth Observation (ITC). Software for remote sensing and GIS.
Jackson, R.B., Moore, L.A., Hoffmann, W.A., Pockman, W.T., Linder, C.R., 1999. Ecosystem rooting depth determined with caves and DNA. Proc. of the Natl. Acad. of Sci. USA 96, 11387–11392.
Kenkmann, T., Schönian, F., 2006. Ries and Chicxulub: impact craters on Earth provide insights for Martian ejecta blankets. Meteorics Planet. Sci. 41 (10), 1587–1603.
Kilroy, G., Coxon, C., Ryan, J., O'Connor, A., Daly, D., 2005. Groundwater and wetland management in the Shannon river basin (Ireland). Environ. Sci. Policy 8, 219–225.
Kiraly, L., 2003. Karstification and groundwater flow. Speleogenesis Evolut. Karst Aquifers 1 (3), 26.
Knochenmus, L.A., Robinson, J.L., 1996. Descriptions of Anisotropy and Heterogeneity and their Effect on Ground-Water Flow and Areas of Contribution to Public Supply Wells in a Karst Carbonate Aquifer System. US Geol. Surv. Water-Supply Pap. 2475, pp. 46. ISBN:0-607-86216-5.
Kovacs, A., Perrochet, P., Király, L., Jeannin, P.-Y., 2005. A quantitative method for the characterisation of karst aquifers based on spring hydrograph analysis. J. Hydrol. 303, 152–164. doi:10.1016/j.jhydrol.2004.08.023.
Krause, S., Heathwaite, A.L., Miller, F., Hulme, P., Crowe, A., 2007. Groundwater-dependent wetlands in the UK and Ireland: controls, functioning and assessing the likelihood of damage from human activities. Water Resour. Manage. 21, 2015–2025. doi:10.1007/s11269-007-9192-x.
Krekeler, M.P.S., Probst, P., Samsonov, M., Tselepis, C.M., Bates, W., Kearns, L.E., Barry Maynard, J., 2007. Investigations of subsurface flow constructed wetlands and associated geomaterial resources in the Akumal and Reforma regions, Quintana Roo. Mexico. Environ. Geol. 53, 709–726. doi:10.1007/s00254-007-0684-z.
Lang, J., Alcolado, P., Carricart-Ganivet, J.P., Chiappone, M., Curran, A., Dustan, P., Gaudian, G., Geraldes, F., Gittings, S., Smith, R., Tunnell, W., Wiener, J., 1998. Status of coral reefs in the northern areas of the wider Caribbean. In: Wilkinson, C. (Ed.), Status of Coral Reefs of the World: 1998. Aust. Inst. of Mar. Sci. Townsv., Aust. (Chapter 8).
Larocque, M., Banton, O., Ackerer, P., Razack, M., 1999. Determining karst transmissivities with inverse modeling and an equivalent porous media. Ground Water 37 (6), 897–903.
Larocque, M., Banton, O., Razack, M., 2000. Transient-state history matching of a karst aquifer ground water flow model. Ground water 38 (6), 939–946.
Li, X., Tsai, F.T.-C., 2009. Bayesian model averaging for groundwater head prediction and uncertainty analysis using multimodel and multimethod. Water Resour. Res. 45, W09403. doi:10.1029/2008WR007488.
Li, G., Loper, D.E., Kung, R., 2008. Contaminant sequestration in karstic aquifers: experiments and quantification. Water Resour. Res. 44, W02429. doi:10.1029/2006WR005797.
Liedl, R., Sauter, M., Hückinghaus, D., Clemens, T., Teutsch, G., 2003. Simulation of the development of karst aquifers using a coupled continuum pipe flow model. Water Resour. Res. 39 (3), SBH61–SBH611.
Lindgren, R.J., Dutton, A.R., Hovorka, S.D., Worthington, S.R.H., Painter, S., 2005. Conceptualization and simulation of the Edwards Aquifer, San Antonio Region, Texas. In: Kuniansky, E. (Ed.), Sci. Investig. Rep. 2005-5160, pp. 48–57.
Lopez-Ramos, E., 1975. Geological summary of the Yucatan Peninsula. In: Nairn, A.E.M., Stehli, F.G. (Eds.), The Ocean Basins and Margins, vol. 3. The Gulf of Mexico and the Caribbean, Plenum Press, NY, USA (Chapter 7).
Luo, Y.F., Peng, S.Z., Khan, S., Cui, Y.L., Wang, Y., Feng, Y.H., 2009. A comparative study of groundwater evapotranspiration functions. In: Anderssen, R.S., Braddock, R.D., Newham, L.T.H. (Eds.), Proc. from the 18th World IMACS Congress and MODSIM09 International Congress on Modelling and Simulation, Cairns, Australia, 13–17 July 2009.
Marín, L.E., Steinich, B., Pacheco, J., Escolero, O.A., 2000. Hydrogeology of a contaminated sole-source karst aquifer, Mérida, Yucatán, Mexico. Geofís. Int. 49 (4), 359–365.
Marshall, L., Sharma, A., Nott, D., 2006. Modeling the catchment via mixtures: issues of model specification and validation. Water Resour. Res. 42, W11409. doi:10.1029/2005WR004613.
Martin, J.B., Screaton, E.J., 2001. Exchange of matrix and conduit water with examples from the Floridan aquifer. In: Kuniansky, E. (Ed.), Water Resources Investigations Report 01-4011, US Geological Survey, pp. 38–44.
Mazzotti, F.J., Fling, H.E., Merediz, G., Lazcano, M., Lasch, C., Barnes, T., 2005. Conceptual ecological model of the Sian Ka'an Biosphere Reserve, Quintana Roo, Mexico. Wetlands 25 (4), 980–997.
McElrone, A.J., Pockman, W.T., Martínez-Vilalta, J., Jackson, R.B., 2004. Variation in xylem structure and function in stems and roots of trees to 20 m depth. New Phytol. 163, 507–517.
Milanović, P.T., 2004. Water Resources Engineering in Karst. CRC Press, Florida, USA (pp. 312, ISBN:1-56670-671-8).
Miller, T.E., 1996. Geologic and hydrologic controls on karst and cave development in Belize. J. Cave Karst Stud. 58 (2), 100–120.
Moore, Y.H., Stoessell, R.K., Easley, D.H., 1992. Fresh-water/sea-water relationship within a ground-water flow system, northeastern coast of the Yucatan Peninsula. Ground Water 30 (3), 343–350.
Morales Barbosa, J.J., 1992. Los humedales, un mundo olvidado. In: Series: Sian Ka'an, Introducción a los Ecosistemas de la Península de Yucatan. Amigos de Sian Ka'an A.C. Impresos MARCA, Mérida, Yucatán, Mexico.

Münch, Z., Conrad, J., 2007. Remote sensing and GIS based determination of groundwater dependent ecosystems in the Western Cape, South Africa. Hydrogeol. J. 15, 19–28. doi:10.1007/s10040-006-0125-1.

Neuman, S.P., 2003. Maximum likelihood Bayesian averaging of uncertain model predictions. Stoch. Environ. Res. Risk Assess. 17, 291–305. doi:10.1007/s00477-003-0151-7.

Neuman, B.R., Rahbek, M.L., 2007. Modeling the Groundwater Catchment of the Sian Ka'an Reserve, Quintana Roo. Assoc. for Mex. Cave Stud. Bull. 18. Austin, TX, USA.

Neuman, S.P., Wierenga, P.J., 2003. A Comprehensive Strategy of Hydrogeologic Modeling and Uncertainty Analysis for Nuclear Facilities and Sites. Univ. of Ariz., Rep. NUREG/CR-6805.

Pacheco, J., Marín, L., Cabrera, A., Steinich, B., Escolero, O., 2001. Nitrate temporal and spatial Patterns in 12 water-supply wells, Yucatan, Mexico. Environ. Geol. 40 (6), 708–715.

Perry, E., Velazquez-Oliman, G., Marin, L., 2002. The hydrogeochemistry of the karst aquifer system of the northern Yucatan Peninsula, Mexico. Int. Geol. Rev. 44, 191–221.

Perry, E., Paytan, A., Pedersen, B., Velazquez-Oliman, G., 2009. Groundwater geochemistry of the Yucatan Peninsula, Mexico: constraints on stratigraphy and hydrogeology. J. Hydrol. 367 (1–2), 27–40. doi:10.1016/j.jhydrol.2008.12.026.

Peterson, E.W., Wicks, C.M., 2005. Fluid and solute transport from a conduit to the matrix in a carbonate aquifer system. Math. Geol. 37 (8), 851–867. doi:10.1007/s11004-005-9211-5.

Peterson, E.W., Wicks, C.M., 2006. Asessing the importance of conduit geometry and physical parameters in karst systems using the storm water management model (SWMM). J. Hydrol. 329, 294–305. doi:10.1016/j.jhydrol.2006.02.017.

Pockman, W.T., McElrone, A.J., Bleby, T.M., Jackson, R.B., 2008. The structure and function of roots of woody species on the Edwards Plateau, Texas, USA, Eos Trans. AGU, 89(23), Jt. Assem. Suppl., Abstract H34A-02.

Pope, K.O., Dahlin, B.H., 1989. Ancient Maya wetland agriculture: new insights from ecological and remote sensing research. J. Field Archeol. 16 (1), 87–106.

Pope, K.O., Ocampo, A.C., Fischer, A.G., Vega, F.J., Ames, D.E., King Jr., D.T., Fouke, B.W., Wachtman, R.J., Kletetschka, G., 2005. Chicxulub impact ejecta deposits in southern Quintana Roo, México, and central Belize. In: Kenkmann, T., Hörz, F., Deutsch, A. (Eds.), Large meteorite impacts III, Geol. Soc. Am. Spec. Pap. 384, pp. 171–190.

Powell, S.J., Letcher, R.A., Croke, B.F.W., 2008. Modelling floodplain inundation for environmental flows: Gwydir wetlands, Australia. Ecol. Modell. 211, 350–362.

Querejeta, J.I., Estrada-Medina, H., Allen, M.F., Jiménez-Osornio, J.J., 2007. Water resource partitioning among trees growing on shallow karst soils in a seasonally dry tropical climate. Oecologia 152, 26–36.

Refsgaard, J.C., Storm, B., 1995. MIKE SHE. In: Singh, V.P. (Ed.), Computer Models in Watershed Hydrology. Water Resour. Publ., Colo., USA, pp. 809–846.

Refsgaard, J.C., van der Sluijs, J.P., Brown, J., van der Keur, P., 2006. A framework for dealing with uncertainty due to model structure error. Adv. Water Resour. 29, 1586–1597.

Refsgaard, J.C., van der Sluijs, J.P., Højberg, A.L., Vanrolleghem, P.A., 2007. Uncertainty in the environmental modeling process – a framework and guidance. Environ. Modell. Softw. 22, 1543–1556. doi:10.1016/j.envsoft.22007.02.004.

Rojas, R., Feyen, L., Dassargues, A., 2008. Conceptual model uncertainty in groundwater modeling: combining generalized likelihood uncertainty estimation and Bayesian model averaging. Water Resour. Res. 44, W12418. doi:10.1029/2008WR006908.

Rojas, R., Feyen, L., Dassargues, A., 2009. Sensitivity analysis of prior model probabilities and the value of prior knowledge in the assessment of conceptual model uncertainty in groundwater modelling. Hydrol. Process. 23, 1131–1146. doi:10.1002/hyp.7231.

Rosencrantz, E., 1990. Structure and tectonics of the Yucatan Basin, Caribbean Sea, as determined from seismic reflection studies. Tectonics 9 (5), 1037–1059.

Sánchez-Sánchez, O., Islebe, G.A., 2002. Tropical forest communities in southeastern Mexico. Plant Ecol. 158, 183–200.

Scanlon, B.R., Mace, R.E., Barrett, M.E., Smith, B., 2003. Can we simulate regional groundwater flow in a karst system using equivalent porous media models? Case study, Barton Springs Edwards Aquifer, USA. J. Hydrol. 276, 137–158 (doi:10.1016/S0022-1694(03)00064-7).

Schönian, F., Stöffler, D., Kenkmann, T., Wittmann, A., 2004. The fluidized Chicxulub ejecta blanket, Mexico: Implications for Mars. In: Poster, 35th Annu. Lunar and Planet. Sci. Conf., Leag. City, TX, USA.

Schönian, F., Tagle, R., Stöffler, D., Kenkmann, T., 2005. Geology of southern Quintana Roo (Mexico) and the Chicxulub ejecta blanket. In: 36th Annu. Lunar and Planet. Sci. Conf., Leag. City, TX, USA. (Abstract #2389).

SGM (Servicio Geológico Mexicano), 2007. Carta Geológica de México. Escala 1:2,000,000. 6ª edición (Geological map of Mexico. Scale 1:2,000000. 6th edition).

Smart, P.L., Beddows, P.A., Coke, J., Doerr, S., Smith, S., Whitaker, F.F., 2006. Cave development on the Caribbean coast of the Yucatan Peninsula, Quintana Roo, Mexico. In: Harmon, R.S., Wicks, C. (Eds.), Perspectives on Karst Geomorphology, Hydrology and Geochemistry – A Tribute Volume to Derek C. Ford and William B. White. Geol. Soc. Am. Spec. Pap. 404, pp. 105–128.

Southworth, C.S., 1985. Applications of remote-sensing data, eastern Yucatan. In: Ward, W.C., Weidie, A.E., Back, W. (Eds.), Geology and Hydrogeology of the Yucatan and Quaternary Geology of Northeastern Yucatan Peninsula. New Orleans Geol. Soc. Publ., New Orleans, LA, USA, pp. 12–19.

Spiessl, S.M., Prommer, H., Licha, T., Sauter, M., Zheng, C., 2007. A process-based reactive hybrid transport model for coupled discrete conduit-continuum systems. J. Hydrol. 347, 23–34.

Stauffer, F., Attinger, S., Zimmermann, S., Kinzelbach, W., 2002. Uncertainty estimation of well catchments in heterogeneous aquifers. Water Resour. Res. 38 (11), 1238. doi:10.1029/2001WR000819.

Stauffer, F., Guadagnini, A., Butler, A., Hendricks Franssen, H.-J., Van de Wiel, N., Bakr, M., Riva, M., Guadagnini, L., 2005. Delineation of source protection zones using statistical methods. Water Resour. Manage. 19, 163–185. doi:10.1007/s11269-005-3482-7.

Stisen, S., Sandholt, I., Nørgaard, A., Fensholt, R., Høegh Jensen, K., 2008. Combining the triangle method with thermal inertia to estimate regional evapotranspiration – applied to MSG-SEVIRI data in the Senegal River basin. Remote Sens. Environ. 112, 1242–1255.

Supper, R., Motschka, K., Ahl, A., Bauer-Gottwein, P., Gondwe, B., Merediz Alonso, G., Römer, A., Ottowitz, D., Kinzelbach, W., 2009. Spatial mapping of submerged cave systems by means of airborne electromagnetics: an emerging technology to support protection of endangered karst aquifers. Near Surf. Geophys. 7 (5), 613–627. doi:10.3997/1873-0604.2009008.

The MathWorks, R2008b. The Software Matlab, Version.

Thomas, C., 1999. Aspects hydrogéologiques du Yucatan (Mexique). Karstologia 34 (2), 9–22.

TNC, 2008. Sian Ka'an Biosphere Reserve. Published on the Website Parks in Peril by The Nature Concervancy (TNC). <http://www.parksinperil.org/wherewework/mexico/protectedarea/siankaan.html> (accessed November 2009).

Urrutia-Fucugauchi, J., Chavez-Aguirre, J.M., Pérez-Cruz, L., De la Rosa, J.L., 2008. Impact ejecta and carbonate sequence in the eastern sector of the Chicxulub crater. C. R. Geosci. 340, 801–810.

USGS, 2006. Shuttle Radar Topography Mission, 3 Arc Second, Finished 2.0. US Geol. Surv. Glob. Land Cover Facil., Univ. of Maryland, College Park, MD, February 2000.

Vacher, H.L., 1988. Dupuit–Ghyben–Herzberg analysis of strip-island lenses. Geol. Soc. Am. Bull. 100 (4), 580–591.

Vassolo, S., Kinzelbach, W., Schäfer, W., 1998. Determination of a well head protection zone by stochastic inverse modelling. J. Hydrol. 206, 268–280.

Weidie, A.E., 1985. Geology of Yucatan Platform. In: Ward, W.C., Weidie, A.E., Back, W. (Eds.), Geology and Hydrogeology of the Yucatan and Quaternary Geology of Northeastern Yucatan Peninsula. New Orleans Geol. Soc. Publ., New Orleans, LA, USA, pp. 1–12.

White, W.B., 1999. Conceptual models for karstic aquifers. In: Palmer, A.N., Palmer, M.V., Sasowsky, I.D. (Eds.), Karst Modeling. The Karst Waters Institute, Charles Town, West Virginia, USA, pp. 11–16 (Spec. Publ. 5).

Worthington, S.R.H., 2003. A comprehensive strategy for understanding flow in carbonate aquifer. Speleogenesis Evol. Karst Aquifers 1 (1), 1–8.

Worthington, S.R.H., 2009. Diagnostic hydrogeologic characteristics of a karst aquifer (Kentucky, USA). Hydrogeol. J. 17, 1665–1678.

Worthington, S.R.H., Ford, D.C., 2009. Self-organized permeability in carbonate aquifers. Ground Water 47 (3), 326–336. doi:10.1111/j.1745-6584.2009.00551.

Xiong, L., Shamseldin, A.Y., O'Connor, K.M., 2001. A non-linear combination of the forecasts of rainfall–runoff models by the first-order Takagi–Sugeno fuzzy system. J. Hydrol. 245, 196–217.